Geophysical Journal International

Geophys. J. Int. (2021) **225,** 1392–1411
Advance Access publication 2021 January 29
GJI Seismology

doi: 10.1093/gji/ggab033

A Bayesian inference framework for fault slip distributions based on ensemble modelling of the uncertainty of underground structure: with a focus on uncertain fault dip

Ryoichiro Agata [1], Amato Kasahara[2] and Yuji Yagi[3]

[1] *Japan Agency for Marine-Earth Science and Technology,* 3173-25 *Showa-machi, Kanazawa-ku, Yokohama* 236-0001*, Japan. E-mail: agatar@jamstec.go.jp*
[2] *Independent researcher*
[3] *Faculty of Life and Environmental Sciences, University of Tsukuba, Tsukuba, Ibaraki* 305-8572*, Japan*

Received 2021 January 12; in original form 2020 July 2

SUMMARY

The model prediction errors that originate from the uncertainty of underground structure are often a major contributor of the errors between the data and the model predictions in fault slip estimation using geodetic or seismic waveform data. However, most studies on slip inversions either neglect the model prediction errors or do not distinguish them from observation errors. Several methods that explicitly incorporated the model prediction errors in slip estimation, which has been proposed in the past decade, commonly assumed a Gaussian distribution for the stochastic property of the model prediction errors to simplify the formulation. Moreover, the information on both the slip distribution and the underground structure is expected to be successfully extracted from the data by incorporating the stochastic property of the model prediction errors. In this study, we propose a novel flexible Bayesian inference framework for estimating fault slips that can accurately incorporate non-Gaussian model prediction errors. This method considers the uncertainty of the underground structure, including fault geometry, based on the ensemble modelling of the uncertainty of Green's functions. Furthermore, the framework allows the estimation of the posterior probability density function (PDF) of the parameters of the underground structure by calculating the likelihood of each sample in the ensemble. We performed numerical experiments for estimating the slip deficit rate (SDR) distribution on a 2-D thrust fault using synthetic data of surface displacement rates, which is the simplest problem setting that can essentially demonstrate the fundamental idea and validate the advantage of the proposed method. In the experiments, the dip angle of the fault plane was the parameter used to characterize the underground structure. The proposed method succeeded in estimating a posterior PDF of SDR that is consistent with the true one, despite the uncertain and inaccurate information of the dip angle. In addition, the method could estimate a posterior PDF of the dip angle that has a strong peak near the true angle. In contrast, the estimation results obtained using a conventional approach, which introduces regularization based on smoothing constraints and does not explicitly distinguish the prediction and observation errors, included a significant amount of bias, which was not noted in the results obtained using the proposed method. The estimation results obtained using different settings of the parameters suggested that inaccurate prior information of the underground structure with a small variance possibly results in significant bias in the estimated PDFs, particularly the posterior PDFs for SDR, those for the underground structure, and the posterior predicted PDF of the displacement rates. The distribution shapes of the model prediction errors for the representative model parameters in certain observation points are significantly asymmetric with large absolute values of the sample skewness, suggesting that they would not be well-modelled by Gaussian approximations.

Key words: Inverse theory; Probability distributions; Earthquake source observations.

1 INTRODUCTION

Estimation of fault slip distributions, including co-seismic slips, aseismic slips and interplate couplings, is an essential step to better understand earthquake generation processes and assess seismic hazards. To estimate fault slip distributions using geodetic or waveform data, the underground fault slip parameters are typically linearly related to the surface geodetic or seismic response at each observation point using a coefficient matrix calculated based on Green's functions, assuming linear elastic media. Green's functions are characterized by the setting of the numerical model for the underground structure (i.e. including, but not limited to, seismic velocity structure and fault geometry). Hereafter, we refer to the parameters for fault slips and those that characterize the underground structure as 'model parameters' and 'underground structure parameters', respectively.

In real-world problems, the values of Green's functions are uncertain because the corresponding underground structure is always uncertain. Because of this uncertainty, the surface responses predicted by combining the fault slip parameters and Green's functions are always associated with model prediction errors relative to the true response. Although ignoring model prediction errors in the inverse problem formulations due to the uncertainty in Green's functions possibly introduces bias into the estimation results, the majority of studies still neglect model prediction errors or do not distinguish them from observation errors in the inverse problem formulations. However, the past decade has seen remarkable progress in the mathematical formulation of model prediction errors due to the uncertainty in Green's functions in earthquake source inversions. The pioneering work of Yagi & Fukahata (2011) proposed an inversion scheme that introduces the error of Green's functions following a Gaussian distribution and iteratively estimates the model parameters and the covariance matrix for the model prediction errors simultaneously. Minson *et al.* (2013) introduced a Gaussian model for describing the model prediction errors, using a diagonal covariance matrix with variances that are positively correlated with the observed amplitudes. Duputel *et al.* (2014) proposed a comprehensive framework to compute the covariance matrix for the model prediction errors based on uncertain and presumably inaccurate prior knowledge of the underground elastic structure, which was later applied to consideration of uncertainty of fault geometry (Ragon *et al.* 2018). Both Minson *et al.* (2013) and Duputel *et al.* (2014) claimed that available fault slip models for the same earthquake are often quite contrasting because of the combination of an inaccurate forward model and subjective regularization of the inverse problem. They tried to resolve this problem based on fully Bayesian inference by developing an accurate stochastic model that better describes the modelling uncertainty in predicting the response at the observation points for geodetic and seismic waveform data. There have also been efforts to estimate a better data covariance with cheaper calculation costs (e.g. Dettmer *et al.* 2007, 2014; Yagi & Fukahata 2008; Hallo & Gallovič 2016; Agata 2020). Other studies have addressed the same issue by estimating the underground structure parameters simultaneously to fault slip estimation (e.g. Fukahata & Wright 2008; Fukuda & Johnson 2010; Minson *et al.* 2014; Agata *et al.* 2018; Vasyura-Bathke *et al.* 2020; Shimizu *et al.* 2021), by seeking to reduce the model prediction errors directly rather than introducing their stochastic properties.

One common feature of the proposed methods in the referred studies herein is that the model prediction errors are assumed to follow a Gaussian distribution. Gaussian distribution is widely used not only because of its maximum entropy property, but also because its use simplifies the analysis of equations, which is necessary for considering the combined effect of prediction and observation errors. The assumption of Gaussianity may be valid when the assumed deviation of the underground structure parameters is sufficiently small, such that the relationship between the predicted response and the parameters is well approximated by linearity (Duputel *et al.* 2014). However, it is difficult to ensure that this approximation has acceptable accuracy for all target problems because we do not have objective criteria with which to define acceptance of the approximation. Moreover, these studies did not extract underground structure information from the observation data. Accurately incorporating the stochastic property of the model prediction errors in fault slip estimation may help in obtaining information about the underground structure in the data.

Consideration of approximating the target probability density function (PDF) using an ensemble of sample models, mainly by Bayesian sampling via Markov chain Monte Carlo (MCMC) methods, has increased flexibility of parameter estimation for fault slip (Fukuda & Johnson 2008, 2010; Minson *et al.* 2013; Dettmer *et al.* 2014; Duputel *et al.* 2014; Ragon *et al.* 2018, and many others). Such ensemble modelling of PDFs has increased the generality of sequential Bayesian inference, which can be interpreted as a type of online inversion method. For example, in the ensemble Kalman filter (EnKF; Evensen 1994), the stochastic variables that need to be evaluated are approximately calculated based on an ensemble of candidate models, which enables Kalman filtering to be applied to weakly nonlinear and larger-scale problems. The particle filter (Gordon *et al.* 1993; Kitagawa 1993, 1996), or, also known as the sequential Monte Carlo method, generates many candidate models (particles) that are sampled from the model space, allowing for further flexible modelling by choosing candidates that are closer to the true model based on the likelihood of each candidate. These methods, both based on ensemble modelling of PDFs, have been widely used in the last few decades with the help of an increasing amount of computation resources. The introduction of such ensemble-based approaches is also expected to bring more flexibility in incorporating the stochastic property of the model prediction errors in fault slip estimation. It may also help to narrow down the parameter space of the candidate underground structure used in fault slip estimation by choosing structures that are more consistent with the data from the ensemble in a similar manner as the particle filter.

This study considers the uncertainty of the underground structure based on ensemble modelling of the uncertainty of Green's functions in estimating fault slip distributions. Such an approach allows for the (1) consideration of the model prediction error more accurately without assuming Gaussianity and (2) extraction of information on not only fault slips but also the underground structure from the data. We set a Bayesian inversion problem and draw samples from the posterior PDF of the fault slip using a type of MCMC method, in which we calculate an integration term that combines the terms of the observation and model prediction errors using the Monte Carlo approximation. This approach enables the estimation of the posterior PDF of the slip distribution, accurately incorporating the stochastic property of the

model prediction errors without assuming Gaussianity. Moreover, because the likelihood for each coefficient matrix is also calculated in the process of performing the Monte Carlo integration, we can simultaneously find underground structure models that are consistent with the observation data. Furthermore, accurate incorporation of the stochastic property of the model prediction errors in a fully Bayesian framework encourages slip estimations without the regularization of smoothing constraints as a prior PDF, as pointed out by Minson *et al.* (2013) and Duputel *et al.* (2014). Numerical experiments are performed in the simplest problem setting allowable for demonstrating the fundamental idea and validating the advantage of the proposed framework: the slip deficit rate (SDR) distribution is estimated on a thrust fault in a 2-D elastic half-space using synthetic data of surface displacement rates, in which the dip angle of the fault plane is the only parameter that characterizes the underground structure. The framework proposed in this study is generally applicable to inverse problems that include parameters characterizing the structure of the media for which only uncertain information is available, similar to the majority of geophysical inverse problems.

This paper is organized as follows: Section 2 describes the formulation of Bayesian inference for fault slips based on ensemble modelling of the uncertainty of the underground structure. Section 3 presents a method for estimating the parameters of an underground structure, while in Section 4, the proposed method is applied to a simple 2-D synthetic test of a geodetic inverse problem. Section 5 discusses several points regarding the application of the proposed method to real-world problems, and finally, Section 6 provides the concluding remarks.

2 FULLY BAYESIAN FORMULATION OF FAULT SLIP ESTIMATION BASED ON ENSEMBLE MODELLING OF THE UNDERGROUND STRUCTURE UNCERTAINTY

2.1 Observation and prediction errors in Bayesian formulation of fault slip estimation

Let us consider an estimation problem of $\mathbf{m}$, a vector for the parameters of slip distribution, or model parameters in a more general viewpoint, using $\mathbf{d}$, a vector for the observation data. We interchangeably use 'fault slip parameters' and 'model parameters'. This estimation problem can be formulated as a Bayesian source inversion, in which we estimate the posterior PDF of $\mathbf{m}$ as

$$P(\mathbf{m}|\mathbf{d}) = \kappa\, P(\mathbf{d}|\mathbf{m})P(\mathbf{m}), \tag{1}$$

where $P(\mathbf{m})$ is the prior PDF of the model parameters, and the conditional PDF $P(\mathbf{d}|\mathbf{m})$ and $P(\mathbf{m}|\mathbf{d})$ are the likelihood function and posterior PDF of the model parameters, respectively. $\kappa = 1/P(\mathbf{d})$ is a normalization factor, which takes a constant value because the observation data and model are fixed. The prior PDF is set based on our prior knowledge of the slip distribution. In addition, a properly defined likelihood function is required for evaluating the posterior PDF. In defining the likelihood function, we relate the data and model parameters in two steps. First, the surface displacement is predicted by the function $\mathbf{g}(\mathbf{m})$. Herein, we consider a linear system, where the prediction is simply made by matrix-vector multiplication, that is, $\mathbf{g}(\mathbf{m}) = \mathbf{G}\mathbf{m}$, where $\mathbf{G}$ is a coefficient matrix calculated based on Green's functions. We denote the predicted response at the observation point by $\mathbf{d}_{\rm pred}$. The stochastic property of the model prediction for a given $\mathbf{m}$, which we call the prediction errors, is described by a conditional PDF $P(\mathbf{d}_{\rm pred}|\mathbf{m})$. The stochastic property of the measurement of the response, which is characterized by the knowledge of the error property of the observation instrument, is denoted by a conditional PDF $P(\mathbf{d}|\mathbf{d}_{\rm pred})$. The likelihood function can then be obtained by marginalizing the product of these two PDFs with $\mathbf{d}_{\rm pred}$ (Duputel *et al.* 2014) as

$$P(\mathbf{d}|\mathbf{m}) = \int P(\mathbf{d}|\mathbf{d}_{\rm pred})P(\mathbf{d}_{\rm pred}|\mathbf{m})\mathrm{d}\mathbf{d}_{\rm pred}. \tag{2}$$

If we assume that both PDFs follow a Gaussian distribution, the integration of eq. (2) can be calculated analytically. Previous studies (e.g. Duputel *et al.* 2014; Ragon *et al.* 2018) made use of this fact and assumed that the prediction errors follow Gaussian distribution to make the formulation and calculation simple and efficient. In contrast, the proposed approach calculates this integration based on Monte Carlo integration using random samples of $\mathbf{d}_{\rm pred}$, without assuming Gaussianity in the prediction errors.

2.2 Calculation of likelihood function based on ensemble modelling of the uncertainty of Green's functions

We assumed that the main source of the prediction errors is the uncertainty of the underground structure, characterized by the underground structure parameters, such as those for the fault geometry and elastic properties, which are denoted by $\boldsymbol{\varphi}$. We consider incorporating the stochastic property of $\boldsymbol{\varphi}$ in the estimation of the model parameters. In the context of Bayesian inversion, $\boldsymbol{\varphi}$ can also be interpreted as hyperparameters in hierarchical Bayesian modelling (Fukahata & Wright 2008) because $\boldsymbol{\varphi}$ controls the distribution of the model parameters (Bishop 2006). We suppose that $P(\boldsymbol{\varphi})$, the stochastic property of the underground structure parameters that is also interpreted as the prior PDF, is already provided based on the existing underground structure models. We draw a significant number of random samples $\boldsymbol{\varphi}^{(n)}$ from $P(\boldsymbol{\varphi})$. Because the coefficient matrix is determined when $\boldsymbol{\varphi}$ is fixed, we can produce an ensemble of matrices consisting of $\mathbf{G}(\boldsymbol{\varphi}^{(n)})$, where $n = 1, \ldots, N$, and N is the ensemble size for the random samples. Here, $\mathbf{G}(\boldsymbol{\varphi}^{(n)})$ means that the coefficient matrix is a (nonlinear) function of the underground structure parameters. We can then straightforwardly calculate the ensemble of $\mathbf{d}_{\rm pred}$, as

$$\{\mathbf{d}^{(1)}_{\rm pred}(\mathbf{m}), \ldots, \mathbf{d}^{(N)}_{\rm pred}(\mathbf{m})\}, \text{ where } \mathbf{d}^{(n)}_{\rm pred}(\mathbf{m}) = \mathbf{G}(\boldsymbol{\varphi}^{(n)})\mathbf{m}\ (n = 1, \ldots, N). \tag{3}$$

$\mathbf{d}^{(n)}_{\mathrm{pred}}(\mathbf{m})$s can be considered as random samples from $P(\mathbf{d}_{\mathrm{pred}}|\mathbf{m})$. Subsequently, Monte Carlo integration can be used to approximate the integration in eq. (2) based on the ensemble of a sufficiently large N as

$$P(\mathbf{d}|\mathbf{m}) \simeq \frac{1}{N}\sum_{n=1}^{N} P(\mathbf{d}|\mathbf{d}^{(n)}_{\mathrm{pred}}(\mathbf{m})). \tag{4}$$

A required ensemble size N is a problem-dependent value. An example of this dependency is presented in the application shown later. For $P(\mathbf{d}|\mathbf{d}_{\mathrm{pred}})$, we require a parametric distribution, whose property is governed by a small number of parameters (see Bishop 2006), to describe the stochastic property of the observation errors. For instance, Gaussian distribution is a widely used parametric distribution to describe the property as

$$P(\mathbf{d}|\mathbf{d}_{\mathrm{pred}}) = (2\pi)^{-N/2}||\mathbf{E}||^{-1/2}\exp\left[-\frac{1}{2}(\mathbf{d}-\mathbf{d}_{\mathrm{pred}})^{\mathrm{T}}\mathbf{E}^{-1}(\mathbf{d}-\mathbf{d}_{\mathrm{pred}})\right], \tag{5}$$

where $\mathbf{E}$ is the covariance matrix that is determined based on the error characteristics of the observation instruments and data processing. When we assume such a parametric distribution of $P(\mathbf{d}|\mathbf{d}_{\mathrm{pred}})$, we can calculate eq. (4). Subsequently, we can then approximate the posterior PDF as

$$P(\mathbf{m}|\mathbf{d}) = \kappa\, P(\mathbf{d}|\mathbf{m})P(\mathbf{m}) \tag{6}$$

$$\simeq \kappa\, \frac{1}{N}\sum_{n=1}^{N} P(\mathbf{d}|\mathbf{d}^{(n)}_{\mathrm{pred}}(\mathbf{m}))P(\mathbf{m}). \tag{7}$$

One advantage of our formulation is that the method is based simply on rigorous mathematical manipulations and the approximation by Monte Carlo integration. To accurately perform Monte Carlo integration, we need to take a sufficiently large ensemble size N, which may increase the associated calculation cost. However, the proposed method can fully account for the association in prediction errors by calculating many matrix-vector products. Consequently, when the number of observation data is increased k times, the proposed method requires only k times larger calculation cost compared to the original problem. This efficiency in time complexity is contrary to that for the previous methods based on the assumption of Gaussianity, in which the covariance matrix for prediction errors is a dense matrix (e.g. Yagi & Fukahata 2011; Duputel *et al.* 2014). Calculation of a dense matrix-vector product required in each step of a sampling algorithm of the posterior PDF generally increases the computation cost k^2 times for a k times larger number of observation data. This discussion is based only on algorithmic complexity. In real problems, the relation of k and N could be more complex (e.g. the sufficient ensemble size for the samples of the underground structure parameters may increase as we obtain more data in some problems settings).

An empirical diagonal matrix is widely used for the covariance matrix $\mathbf{E}$ in eq. (5). Although a detailed discussion on the proper choice of $\mathbf{E}$ is beyond the scope of this study, one can alternatively introduce non-diagonal matrices for $\mathbf{E}$ that describe the correlations between the observation errors considering the data distribution and the characteristics of the observations (e.g. Fukahata & Wright 2008; Iinuma *et al.* 2017). We again emphasize that the choice of $P(\mathbf{d}|\mathbf{d}_{\mathrm{pred}})$ is not limited to Gaussian distribution, and we can incorporate any parametric distribution into the formulation.

2.3 Sampling algorithm for the posterior probability density function of fault slips

We use the replica-exchange Monte Carlo method (REMC; Swendsen & Wang 1986; Geyer 1991), also known as parallel tempering, a type of the MCMC method (Metropolis *et al.* 1953), to perform Bayesian sampling from the target posterior PDF. REMC is capable of drawing samples from the target PDF much more efficiently than simpler MCMC algorithms such as the Metropolis method (Metropolis *et al.* 1953), by performing several samplings with different PDFs characterized by varying 'temperatures' in parallel, between which the samples are randomly exchanged every several time steps. To perform REMC, we use an algorithm that is similar to that used in Kano *et al.* (2017), a recent application example of the method to seismology. Algorithm 1 shows details of the algorithm. If L, the number of chains, is taken to be 1, and the exchange of the samples is not performed, this algorithm becomes identical to that of the Metropolis method. In our applications, the temperature is assumed to be $T_l = a^{l-1}(l = 1, \ldots, L)$, where a is a positive real number and $T_1 = 1$, which means $P_1(\mathbf{m}) = P(\mathbf{m}|\mathbf{d})$. a and other constants used in Algorithm 1 are adjusted so that the acceptance and exchange rate (i.e. the rate for the conditional branch $\star$ and $\star\star$ in Algorithm 1 to be true, respectively) become preferable and the target PDF is sampled properly (see Section 4.1).

3 ESTIMATION OF THE POSTERIOR PDF OF THE UNDERGROUND STRUCTURE PARAMETERS

In the previous section, only the posterior PDF of the model parameters was estimated using the observation data. However, data may also contain information about the underground structure parameters. Herein, we discuss the estimation of the posterior PDF of the underground structure parameters regarding an underground structure in the post-process of Bayesian sampling of the model parameters.

Algorithm 1 The algorithm of REMC used in this study based on Kano et al. (2017). $M_{\text{iteration}}$, M_{burnin}, M_{exchange}, L, $\mathbf{m}_l^{(m)}$, T_l, K, and β_k are the number of iteration, that of the samples for burn-in period, that of the iterations every of which the chains are exchanged, that of the chains, the model parameter in the lth chain at the mth step, the temperature in the lth chain, the number of the model parameters, and the standard deviation of the kth model parameter. $U(a, b)$ denotes a uniform probability distribution from a to b. Mod$(\cdot, \cdot)$ denotes the Modulo operator. The acceptance and the exchange rate are defined as the rate for the conditional branch $\star$ and $\star\star$ to be true.

Input: $M_{\text{iteration}}$, M_{burnin}, M_{exchange}, L, $\mathbf{m}_l^{(0)}$, T_l $(l = 1, \ldots, L)$, K, β_k $(k = 1, \ldots, K)$
Output: $\mathbf{m}_1^{(m)}(m = M_{\text{burnin}}, \ldots, M_{\text{iteration}})$ as the samples drawn from the target PDF
$P_l(\mathbf{m}) = P(\mathbf{m}|\mathbf{d})^{1/T_l}(l = 1, \ldots, L)$ (Define a family of PDFs)
for $m = 0$ to $M - 1$ **do**
  $\mathbf{m}_l^* \Leftarrow \mathbf{m}_l^{(m)} + \boldsymbol{\pi}_l$, $\boldsymbol{\pi}_l \sim N(\mathbf{0}, \text{diag}(\beta_k^2))$
  $P_l^{\text{accept}} \Leftarrow \min\left[1, \dfrac{P_l(\mathbf{m}_l^*)}{P_l(\mathbf{m}_l^{(m)})}\right]$
  $u_l \Leftarrow$ (a random sample from $U(0, 1)$)
  if $u_l \leq P_l^{\text{accept}}$ $\star$ **then**
    $\mathbf{m}_l^{(m+1)} \Leftarrow \mathbf{m}_l^*$
  else
    $\mathbf{m}_l^{(m+1)} \Leftarrow \mathbf{m}_l^{(m)}$
  end if
  } Work in parallel for $l = 1, \ldots, L$
  if Mod$(m, M_{\text{exchange}}) = 0$ **then**
    $u \Leftarrow$ (a random sample from $U(0, 1)$)
    Select randomly a pair of consecutive lth and (l+1)th chains
    $P_{\text{accept}} \Leftarrow \min\left[1, \dfrac{P_l(\mathbf{m}_{l+1}^{(m)})P_{l+1}(\mathbf{m}_l^{(m)})}{P_l(\mathbf{m}_l^{(m)})P_{l+1}(\mathbf{m}_{l+1}^{(m)})}\right]$
    if $u \leq P_{\text{accept}}$ $\star\star$ **then**
      $\mathbf{m}_{l+1}^{(m)} \Leftarrow \mathbf{m}_l^{(m)}$
      $\mathbf{m}_l^{(m)} \Leftarrow \mathbf{m}_{l+1}^{(m)}$
    end if
  end if
  } Exchange samples
end for

3.1 Interpretation of the proposed algorithm in the view of the estimation of joint probability for the model and underground structure parameters

Before discussing the posterior PDF for the underground structure parameters, we consider the joint posterior PDF of the model or slip parameters and the underground structure parameters of the underground structure after obtaining the data, which can be formulated based on Bayes' theorem as

$$P(\mathbf{m}, \boldsymbol{\varphi}|\mathbf{d}) = \kappa\, P(\mathbf{d}|\mathbf{m}, \boldsymbol{\varphi})P(\mathbf{m}, \boldsymbol{\varphi}). \tag{8}$$

For simplicity, we hereafter consider a case where the prior information of $\mathbf{m}$ and $\boldsymbol{\varphi}$ are independent, that is, $P(\mathbf{m}, \boldsymbol{\varphi}) = P(\mathbf{m})P(\boldsymbol{\varphi})$, although the applicability of the method is not limited to such a case. The marginal posterior PDF of $\mathbf{m}$ can be obtained by marginalizing eq. (8) with $\boldsymbol{\varphi}$ as

$$P(\mathbf{m}|\mathbf{d}) = \kappa \int P(\mathbf{d}|\mathbf{m}, \boldsymbol{\varphi})P(\mathbf{m})P(\boldsymbol{\varphi})\mathrm{d}\boldsymbol{\varphi}. \tag{9}$$

If we draw random samples $\boldsymbol{\varphi}^{(n)}$ from $P(\boldsymbol{\varphi})$, eq. (9) can be approximately evaluated based on Monte Carlo integration as

$$P(\mathbf{m}|\mathbf{d}) = \kappa \int P(\mathbf{d}|\mathbf{m}, \boldsymbol{\varphi})P(\mathbf{m})P(\boldsymbol{\varphi})\mathrm{d}\boldsymbol{\varphi} \tag{10}$$

$$\simeq \kappa \frac{1}{N}\sum_{n=1}^{N} P(\mathbf{d}|\mathbf{m}, \boldsymbol{\varphi}^{(n)})P(\mathbf{m}). \tag{11}$$

By comparing this equation with eq. (7), we find that $P(\mathbf{d}|\mathbf{d}_{\text{pred}}^{(n)}(\mathbf{m})) = P(\mathbf{d}|\mathbf{m}, \boldsymbol{\varphi}^{(n)})$. In Section 2, we present the proposed algorithm from the viewpoint of the mathematical formulation of the prediction errors. However, the same algorithm can also be interpreted as the marginalization of a posterior joint probability using the underground structure parameters. The latter interpretation is useful for deriving the formula for estimating the posterior PDF of the underground structure parameters. The marginal posterior PDF of $\mathbf{m}$ can also be estimated by first drawing the joint PDF of $\mathbf{m}$ and $\boldsymbol{\varphi}$ in the left-hand side of eq. (8) using MCMC, and then marginalizing the PDF with $\boldsymbol{\varphi}$, which we call the 'naive approach'. Fig. 1 summarizes the difference between the proposed and naive approach. Advantages and disadvantages of the proposed method over the naive approach are discussed in Section 3.3.

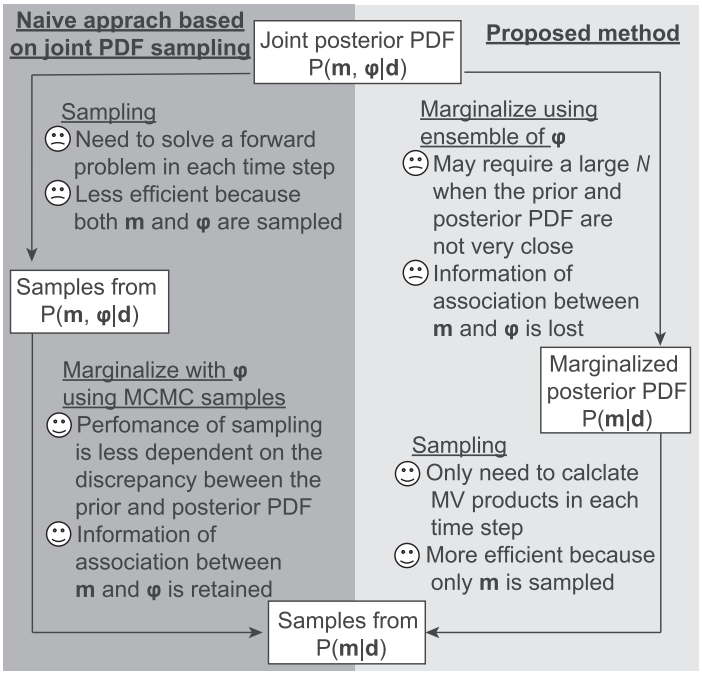

Figure 1. Summary of the comparison the proposed method and a naive approach based on Bayesian sampling from the joint PDF in performing Bayesian sampling of $P(\mathbf{m}|\mathbf{d})$.

3.2 Calculation of the posterior PDF of the underground structure parameters

We obtain the posterior PDF of $\boldsymbol{\varphi}$ by marginalizing eq. (8) with $\mathbf{m}$, which can be further transformed as

$$P(\boldsymbol{\varphi}|\mathbf{d}) = \int P(\mathbf{m}, \boldsymbol{\varphi}|\mathbf{d})\mathrm{d}\mathbf{m} \tag{12}$$

$$= \int P(\boldsymbol{\varphi}|\mathbf{m}, \mathbf{d})P(\mathbf{m}|\mathbf{d})\mathrm{d}\mathbf{m} \tag{13}$$

$$= \int \frac{P(\mathbf{d}|\mathbf{m}, \boldsymbol{\varphi})P(\boldsymbol{\varphi}|\mathbf{m})}{\int P(\mathbf{d}|\mathbf{m}, \boldsymbol{\varphi}')P(\boldsymbol{\varphi}'|\mathbf{m})\mathrm{d}\boldsymbol{\varphi}'} P(\mathbf{m}|\mathbf{d})\mathrm{d}\mathbf{m}, \tag{14}$$

where we use the relations $P(\boldsymbol{\varphi}|\mathbf{m}, \mathbf{d}) = P(\mathbf{d}|\mathbf{m}, \boldsymbol{\varphi})P(\boldsymbol{\varphi}|\mathbf{m})/P(\mathbf{d}|\mathbf{m})$ and $P(\mathbf{d}|\mathbf{m}) = \int P(\mathbf{d}|\mathbf{m}, \boldsymbol{\varphi}')P(\boldsymbol{\varphi}'|\mathbf{m})d\boldsymbol{\varphi}'$ in the transformation from eqs (13) to (14). Suppose we have obtained M ($=M_{\mathrm{iteration}} - M_{\mathrm{burnin}}$ using the constants defined in Algorithm 1) samples from $P(\mathbf{m}|\mathbf{d})$ using the sampling algorithm presented in Section 2.3, then, because $P(\boldsymbol{\varphi}|\mathbf{m}) = P(\boldsymbol{\varphi})$ in the present problem, we can rewrite the equation and approximately calculate $P(\boldsymbol{\varphi}|\mathbf{d})$ based on the Monte Carlo integration as

$$P(\boldsymbol{\varphi}|\mathbf{d}) = \int \frac{P(\mathbf{d}|\mathbf{m}, \boldsymbol{\varphi})P(\boldsymbol{\varphi})}{\int P(\mathbf{d}|\mathbf{m}, \boldsymbol{\varphi}')P(\boldsymbol{\varphi}')\mathrm{d}\boldsymbol{\varphi}'} P(\mathbf{m}|\mathbf{d})\mathrm{d}\mathbf{m} \tag{15}$$

$$\simeq \frac{1}{M}\sum_{m=1}^{M} \frac{P(\mathbf{d}|\mathbf{m}^{(m)}, \boldsymbol{\varphi})P(\boldsymbol{\varphi})}{\frac{1}{N}\sum_{n=1}^{N} P(\mathbf{d}|\mathbf{m}^{(m)}, \boldsymbol{\varphi}^{(n)})}, \tag{16}$$

where the approximation is performed based on the Monte Carlo integration using the samples of $\mathbf{m}$ from $P(\mathbf{m}|\mathbf{d})$ for $\int \mathrm{d}\mathbf{m}$ and $\boldsymbol{\varphi}$ from $P(\boldsymbol{\varphi})$ for $\int \mathrm{d}\boldsymbol{\varphi}'$, respectively. $P(\boldsymbol{\varphi})$ can be approximated using the same N samples of $\boldsymbol{\varphi}$ as those used in eqs (3) and (11), and others by, for example, an approximation based on the Monte Carlo method as

$$\hat{P}(\boldsymbol{\varphi}) = \frac{1}{N}\sum_{n=1}^{N} \delta(\boldsymbol{\varphi} - \boldsymbol{\varphi}^{(n)}), \tag{17}$$

where $\delta(\boldsymbol{\varphi} - \boldsymbol{\varphi}^{(n)})$ is a delta function that satisfies

$$\delta(\mathbf{x}) = \mathbf{0} \ (\mathbf{x} \neq \mathbf{0}), \tag{18}$$

and

$$\int_{\mathbf{S}} f(\mathbf{x})\delta(\mathbf{x} - \mathbf{x}^*)\mathrm{d}\mathbf{x} = \begin{cases} f(\mathbf{x}^*) & (\mathbf{x}^* \in \mathbf{S}) \\ 0 & (\mathbf{x}^* \notin \mathbf{S}). \end{cases} \tag{19}$$

By substituting this term into $P(\boldsymbol{\varphi})$ in eq. (16), the marginal posterior PDF of $\boldsymbol{\varphi}$ can also be written based on the approximation by the Monte Carlo method as

$$\hat{P}(\boldsymbol{\varphi}|\mathbf{d}) = \frac{1}{N}\sum_{n=1}^{N} w^{(n)}\delta(\boldsymbol{\varphi} - \boldsymbol{\varphi}^{(n)}), \tag{20}$$

where

$$w^{(n)} = \frac{1}{M}\sum_{m=1}^{M} \frac{P(\mathbf{d}|\mathbf{m}^{(m)}, \boldsymbol{\varphi}^{(n)})}{\frac{1}{N}\sum_{n'=1}^{N} P(\mathbf{d}|\mathbf{m}^{(m)}, \boldsymbol{\varphi}^{(n')})}. \tag{21}$$

Eq. (20) has the form of importance sampling (Bishop 2006), in which larger weights are placed on the samples for which the probability density is large. Importance sampling is known to be more or at least equally efficient in approximating a distribution compared to the ordinary approximation used in eq. (17). Because $P(\mathbf{d}|\mathbf{m}^{(m)}, \boldsymbol{\varphi}^{(n)})$ is calculated when MCMC sampling for $P(\mathbf{m}|\mathbf{d})$ is performed, as shown in eq. (11), we can readily calculate eq. (20). We herein present a particle approximation based on the delta function to approximate $P(\boldsymbol{\varphi}|\mathbf{d})$ for simplicity, which allows for the drawing of a histogram that represents $P(\boldsymbol{\varphi}|\mathbf{d})$. Applying the kernel density estimation (Rosenblatt 1956), in which a smoother kernel function such as the Gaussian function is used instead of the delta function in eqs (17) and (20), produces an approximated PDF with a smoother distribution.

3.3 Advantages and disadvantages over the naive approach of estimating the joint probability of fault slip and underground structure

Section 2 presents an algorithm for Bayesian sampling of the posterior PDF of the model parameters considering the prediction errors that originated from the uncertainty of the underground structure parameters. The discussion in this section so far suggests that the proposed approach for the model parameter estimation is mathematically equivalent to the estimation based on Bayesian sampling of the joint posterior probability of both the model and underground structure parameters. This would be in terms of using the prior PDF that describes the stochastic properties of the underground structure parameters, followed by marginalizing the joint probability with the underground structure parameters, which can be achieved as long as the Monte Carlo approximations are met in both approaches. Therefore, the difference between the two approaches is whether the target PDF has been marginalized before or after the sampling process. In the context of earthquake source inversions, such a relationship between these two approaches suggests that simultaneous estimation of the parameters for fault slip and the underground structure (e.g. Fukahata & Wright 2008; Fukuda & Johnson 2010; Agata *et al.* 2018) is closely related to fault slip inversion methods considering the prediction errors that originate from the uncertainty of the underground structure (e.g. Yagi & Fukahata 2011; Duputel *et al.* 2014; Ragon *et al.* 2018). Although these two classes of studies clearly address the same problem using similar approaches, the studies categorized in one class often do not refer to those in the other. Because of this close relationship and similarity between the approaches, it is important to point out the practical advantage of the proposed method over the naive approach, in which samples are drawn from the joint PDF of $\mathbf{m}$ and $\boldsymbol{\varphi}$ first and then marginalized with $\boldsymbol{\varphi}$ after the sampling process. Fig. 1 summarizes the difference between the two approaches. There are two major advantages of the proposed method over the naive approach, as discussed below.

First, the computation cost in each step of Bayesian sampling is significantly different in the two approaches. Because the relationship between the underground structure parameters $\boldsymbol{\varphi}$ and the measurement is typically nonlinear, the estimation of the joint posterior probability of $\mathbf{m}$ and $\boldsymbol{\varphi}$ is typed as a nonlinear inversion problem, which requires solving the forward problem in each step of the sampling algorithm to evaluate the target PDF. In contrast, the proposed method marginalizes the likelihood function with the underground structure parameters and deletes them from the equation in advance of Bayesian sampling. This manner reduces the target parameter space for Bayesian sampling to only that of the model parameters, which are in a linear relationship with the measurement, allowing for evaluating the target PDF simply by performing multiple matrix-vector multiplications in eq. (3) to perform Monte Carlo integration in eq. (4). Thus, if the coefficient matrices composed of Green's functions are calculated in advance of the sampling, the sampling process itself only requires relatively simple and cheap calculations. Furthermore, because each component of the coefficient matrix can be calculated independently, the use of a larger-scale computer allows for highly parallelized calculations in preparing the matrix. Sampling from a posterior distribution in a typical application in the field of geophysics in the literature generally requires at least 10^5 sequential evaluations of the target posterior PDF and usually more than that. Furthermore, as mentioned in Section 2.3, MCMC or REMC sampling requires several preliminary runs in order to adjust the parameters for the proposal distributions and temperatures, with which the target PDF is properly sampled. In a problem with relatively small calculation cost for forward modelling, such as the application example in Section 4, running the sampling algorithm based on the naive approach many times for trial and error is not problematic. However, once the calculation cost required for the forward problem is significantly large, each run of the sampling takes a significantly longer amount of time, making a more practical application difficult. For instance, Yamaguchi *et al.* (2017) calculated 1,000 sets of the coefficient matrix for a 3-D heterogeneous underground structure based on finite element modelling in 17 days, which corresponds to 3.6×10^5 executions of the forward problem, using a highly tuned computation program and 64 GPUs. It is impossible to spend the equivalent amount of time and resources to run the same amount of forward problems in performing one trial of sampling.

Second, because the underground structure parameters are usually nonlinearly related to the data, the joint posterior PDF may become a strongly multimodal distribution, thus requiring more sequential evaluations in the sampling process and resulting in difficulty in adjusting

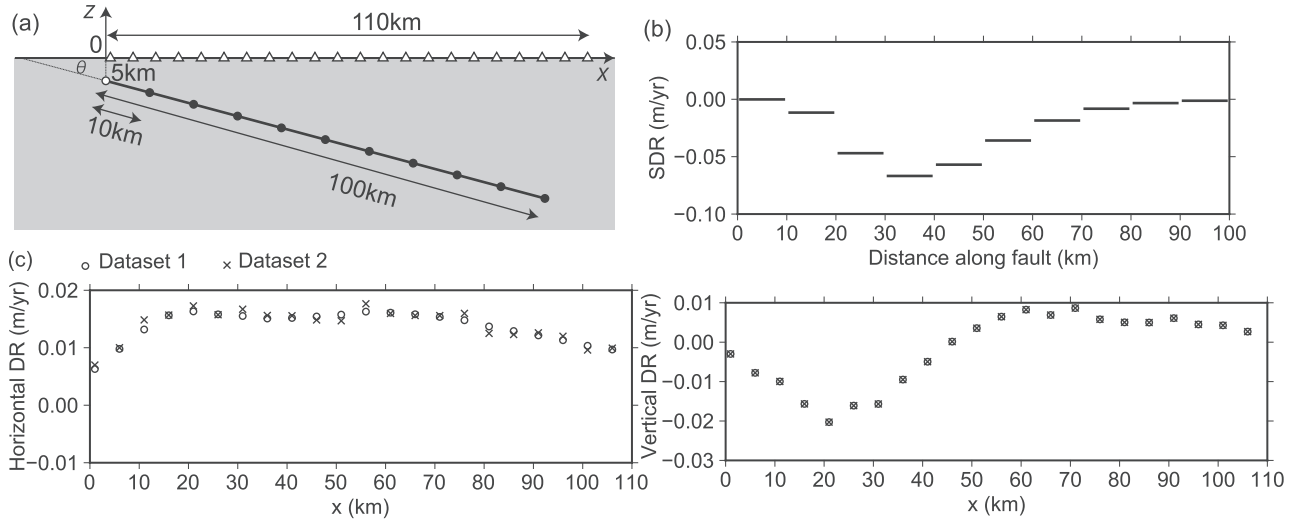

Figure 2. Problem setting of the synthetic tests. (a) Fault geometry. The black dots, white dot and white triangles denote the boundaries of the small faults, the fixed point and the observation point, respectively. The entire fault width and small fault width are taken to be 100 and 10 km, respectively. The true dip angle of the fault $\theta = 15^\circ$. (b) The true SDR distribution inputted on the fault plane. A constant value is taken in each small fault. (c) The synthetic data of displacement rate (DR) in Datasets 1 and 2 calculated based on the true SDR distribution and the fault geometry. Gaussian noises are added to the calculated DR. The data in the two data sets in the vertical component overlap because their difference is only in the amount of the observation errors in the horizontal component.

the parameters to determine the proposal distributions and temperatures in the sampling algorithm. Therefore, the efficiency of Bayesian sampling is expected to be significantly improved if the sampling algorithm explores only the model parameter space. The proposed method allows for sampling only from the model parameter space by marginalizing and removing the underground structure parameter from the PDF in advance of the sampling process. It should be noted that avoiding naive sampling from both spaces of the model and underground structure parameters has been an important issue in previous studies. For instance, Malinverno & Briggs (2004) and Fukuda & Johnson (2010) utilized the linear relationship between the model parameters and the measurement to develop an efficient sampling algorithm from the joint PDF, thus separating the linear and nonlinear parts of the estimation problem. Their approach still required Bayesian sampling from a parameter space which has a nonlinear relationship with the measurement. Therefore, because the underground structure parameters characterized the forward model prediction, it was still necessary to solve the forward problem for each step of the iterative sampling algorithm. For problems in which the computation cost for the forward problem is moderate, their approach should also be effective.

One drawback of the proposed method is that a relatively large number of random samples may be required for the underground structure parameters in a problem setting where the prior and posterior PDF for the underground structure parameters are not close. In such a situation, the ensemble from the prior PDF for $\boldsymbol{\varphi}$ may end up excluding samples that could sufficiently represent the property of the posterior PDF unless we draw an enormous number of random samples from the prior PDF (see Section 4.2.4). In this way, the proposed method may be not competitive with the naive approach, even in terms of net computation cost, because the performance of the naive approach, in which samples are directly drawn from the posterior, is less dependent on the amount of discrepancy between the prior and posterior PDF. Additionally, information on the associations between $\mathbf{m}$ and $\boldsymbol{\varphi}$ cannot be obtained when the proposed method is used, although we expect that it would be difficult to practically handle this information and produce a geophysically meaningful discussion.

4 APPLICATION TO A TOY MODEL PROBLEM OF GEODETIC SLIP ESTIMATION

In this section, we present numerical experiments in the simplest problem setting allowable for demonstrating the fundamental idea and validates the advantage of the proposed framework. A 2-D synthetic test of a geodetic inversion problem that includes a significant amount of prediction errors is performed. Through this example, we demonstrate the capability of the proposed method in estimating the fault slip distribution in a situation in which information about the underground structure is uncertain.

4.1 Problem setting

We consider an estimation problem of the SDR on a dip-slip fault embedded in a 2-D elastic homogeneous half-space, which models a thrust fault. The fault geometry is shown in Fig. 2(a), where the fault width is considered to be 100 km. The top of the fault plane is fixed at the point $(x, z) = (0\,\text{km}, -5\,\text{km})$, and the dip angle controls the fault geometry. The true dip angle of the fault is considered to be 15°. The true SDR distribution shown in Fig. 2(b) is inputted in the fault plane, which is then divided into ten small faults of 10 km width (i.e. $K = 10$), each with a constant slip. The virtual observation points are distributed on the surface of the half-space, which mimics geodetic

Table 1. Parameters for the REMC sampling performed for the base case.

$M_{\text{iteration}}$	M_{burnin}	M_{exchange}	L	a	β_{k}
500 000	10 000	10	20	2	3.0×10^{-4} m yr^{-1}

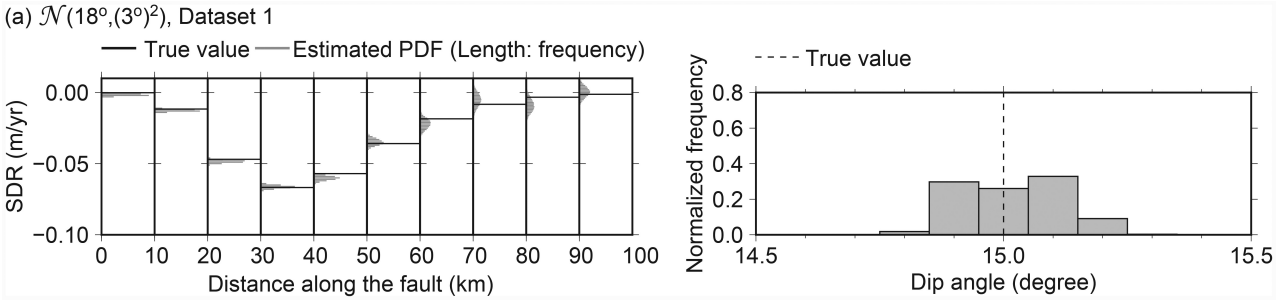

Figure 3. The estimation result in the base case, using Dataset 1 and assuming that θ follows $\mathcal{N}(18^\circ, (3^\circ)^2)$. The left- and right-hand panels show the estimation result of the posterior PDF of SDR and the dip angle, respectively.

observation of the interseismic surface displacement rate (DR). We add artificial Gaussian noise to the calculated displacements, for which the standard deviations are 1.0×10^{-4} m yr^{-1} for the horizontal component and 1.0×10^{-3} m yr^{-1} for the vertical component. We also consider an additional case with larger observation errors, in which the standard deviation for the horizontal component is 1.0×10^{-3} m yr^{-1}. We call the data set in the former case Dataset 1 and that in the latter Dataset 2. Dataset 2 is used only in the problems in Section 4.2.2. Fig. 2(c) illustrates the two synthetic data sets in the observation points. The covariance matrix $\mathbf{E}$ for the observation errors is constructed based on these values of standard deviations.

In estimating the posterior PDF of the SDR distribution, we assume a scenario wherein only uncertain and inaccurate information of the dip angle is available. That is, θ is assumed to be a variable following Gaussian distribution with a mean of 18° and the standard deviation 3° (i.e. $\mathcal{N}(18^\circ, (3^\circ)^2)$), which corresponds to the prior PDF of $\boldsymbol{\varphi}$ or $P(\boldsymbol{\varphi})$ (i.e. $\boldsymbol{\varphi} = \varphi = \theta$). Note that the uncertainty of θ is defined in terms of the angular measure for simplicity, but it is also possible to use other measures to avoid oversampling of shallow dipping faults particularly when considering both the strike and dip angles (e.g. Minson *et al.* 2014). The uncertainty and inaccuracy of $\boldsymbol{\varphi}$ are the sources of prediction errors in this estimation problem. From this PDF, we draw random samples of size $N = 1000$ for the dip angle, denoted as $\{\theta^{(1)} \ldots \theta^{(1000)}\}$, and calculate the ensemble of the coefficient matrices $\{\mathbf{G}(\boldsymbol{\theta}^{(1)}) \ldots \mathbf{G}(\boldsymbol{\theta}^{(1000)})\}$ based on the samples. Samples with a dip angle that is either negative or larger than 90° are simply rejected (note that the same approach is used in the experiments presented hereafter). We use $U(-0.15\,\text{m yr}^{-1}, 0.01\,\text{m yr}^{-1})$ for SDR in each small fault as the prior PDF $P(\mathbf{m})$, where $U(a, b)$ denotes a uniform probability distribution from a to b. Therefore, the specific form of the approximation of the posterior PDF for the model parameter shown in eq. (11) is written as

$$P(\mathbf{m}|\mathbf{d}) \simeq \kappa \frac{1}{N} \sum_{n=1}^{N} P(\mathbf{d}|\mathbf{m}, \boldsymbol{\varphi}^{(n)}) P(\mathbf{m}) \tag{22}$$

$$= \kappa \frac{1}{1000} \sum_{n=1}^{1000} P(\mathbf{D}|\mathbf{m}, \theta^{(n)}) U(-0.15\,\text{m yr}^{-1}, 0.01\,\text{m yr}^{-1})^{10}, \tag{23}$$

where $\mathbf{D}$ is the observation data used for estimating the posterior PDF of the SDR. We do not impose a strong assumption of the characteristic of spatial SDR distribution, such as regularization of a smoothness constraint (e.g. Yabuki & Matsu'ura 1992). We calculate both the synthetic data and the coefficient matrices based on the analytical expression of elastic deformation due to a dipping fault embedded in a 2-D elastic half-space as described in Segall (2010). Based on the synthetic data, the covariance matrix for the observation errors, and the ensemble of the coefficient matrices, we perform REMC sampling of the posterior PDF using the parameters. We adopt the parameters for REMC sampling presented in Table 1, with which the acceptance and the exchange rate fall between 20 and 60 per cent.

4.2 Results

Fig. 3 shows the sampled posterior PDF. In the left-hand panel, smaller variances in the shallower part of the fault and larger ones in the deeper part are seen in the estimated PDF of SDR. Despite that the prior information on the dip angle is inaccurate and uncertain, the true value of SDR falls within the range of the estimated PDFs, which indicates that the stochastic property of the parameters estimated by the proposed method is mathematically consistent with the synthetic data. The right-hand panel shows the weighted histogram consisting of 1,000 samples that approximate the posterior PDF of θ. 88.6 per cent of the samples with weight fall within $\theta = 14.85^\circ$ and 15.15°. It follows that the value of the dip angle is correctly estimated with small uncertainty. Fig. 4 shows the posterior predicted distribution based on the samples from the posterior PDF. A plot of the posterior predicted distribution is produced based on the equation below:

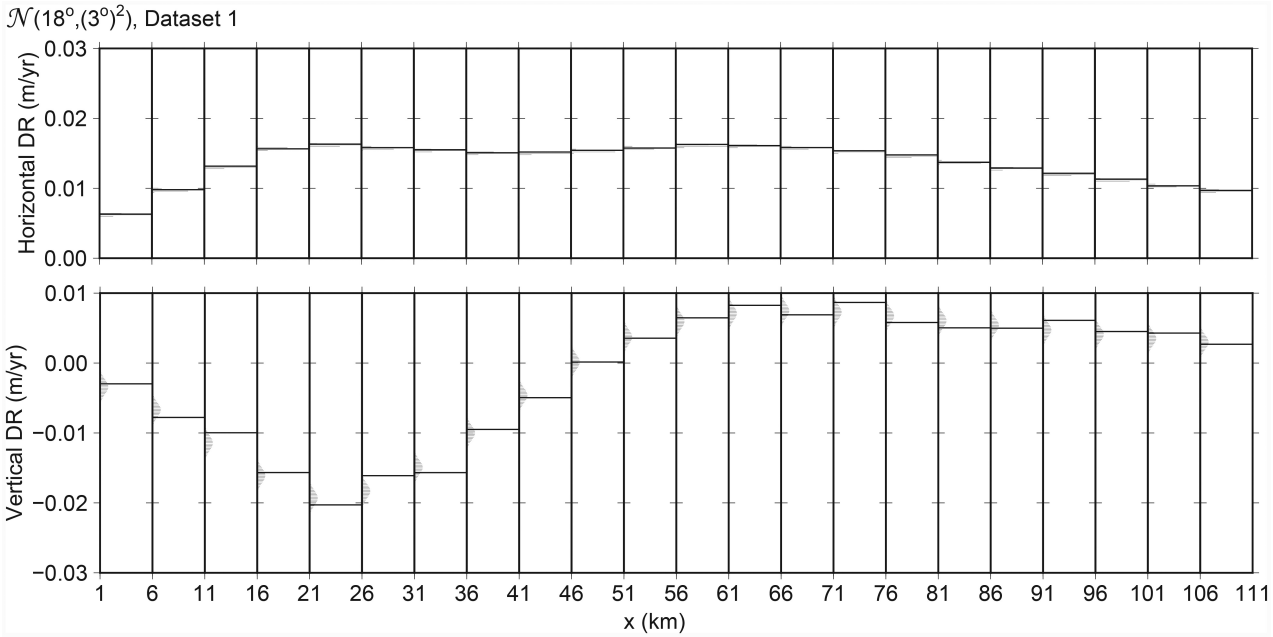

Figure 4. The posterior predicted PDF of horizontal and vertical displacement rate (DR) in the base case, using Dataset 1 and assuming that θ follows $\mathcal{N}(18^\circ, (3^\circ)^2)$.

$$P(\mathbf{d}|\mathbf{D}) = \int\int P(\mathbf{d}|\mathbf{m},\boldsymbol{\varphi})P(\mathbf{m},\boldsymbol{\varphi}|\mathbf{D})\mathrm{d}\mathbf{m}\mathrm{d}\boldsymbol{\varphi} \tag{24}$$

$$\simeq \frac{1}{M}\sum_{m=1}^{M}\int P(\mathbf{d}|\mathbf{m}^{(m)},\boldsymbol{\varphi})\frac{P(\mathbf{D}|\mathbf{m}^{(m)},\boldsymbol{\varphi})P(\boldsymbol{\varphi})}{\frac{1}{N}\sum_{n=1}^{N}P(\mathbf{D}|\mathbf{m}^{(m)},\boldsymbol{\varphi}^{(n)})}\mathrm{d}\boldsymbol{\varphi} \tag{25}$$

$$\simeq \frac{1}{NM}\sum_{n=1}^{N}\sum_{m=1}^{M}P(\mathbf{d}|\mathbf{m}^{(m)},\boldsymbol{\varphi}^{(n)})\frac{P(\mathbf{D}|\mathbf{m}^{(m)},\boldsymbol{\varphi}^{(n)})}{\frac{1}{N}\sum_{n'=1}^{N}P(\mathbf{D}|\mathbf{m}^{(m)},\boldsymbol{\varphi}^{(n')})}, \tag{26}$$

where $P(\mathbf{m},\boldsymbol{\varphi}|\mathbf{D})$ is the joint posterior PDF of the model and underground structure parameters obtained using $\mathbf{d}=\mathbf{D}$. After performing the REMC sampling, the value of $P(\mathbf{D}|\mathbf{m}^{(m)},\boldsymbol{\varphi}^{(n)}) = P(\mathbf{D}|\mathbf{d}^{(n)}_{\mathrm{pred}}(\mathbf{m}^{(m)}))$ for each sample with the indices m and n is already available (see eq. (11) and the explanation therein). The approximation from eqs (24) to (25) is similar to the one used to obtain eqs (16) from (12). The approximation from eqs (25) to (26) is based on Monte Carlo integration for $\boldsymbol{\varphi}$. As the figure shows, the synthetic observation data fall within the range of the predicted distribution. We consider this problem setting as the base case and perform comparisons with several different settings, aiming for detailed discussions.

4.2.1 Robustness of the estimation result versus different assumptions on the mean value of the underground structure parameters—comparison with a conventional approach based on implicit consideration of prediction errors

Here, we estimate the posterior PDF of the SDR based on a different assumption of the mean value of the dip angle and examine the difference in the estimation result. Fig. 5(a) shows the results in the case where θ follows $\mathcal{N}(12^\circ, (3^\circ)^2)$ and Dataset 1 is used. The estimated PDF appears almost identical to that obtained in the base case shown in Fig. 3(a). It follows that accurate consideration of the effect of the prediction errors on the slip estimation leads to similar estimation results despite the difference in the assumption on the mean value of the prior PDF for the dip angle.

We additionally compare the estimation results obtained using the proposed method and those based on a conventional approach which does not explicitly distinguish the prediction errors from the observation errors. For instance, such an approach is taken in combination with smoothing constraints in widely applied inversion analysis methods of slip distribution (e.g. Yabuki & Matsu'ura 1992). In such methods, the use of a smoothing constraint introduces a penalty due to the spatial roughness of the slip distribution to the evaluation function. To perform an estimation with a prior constraint on the smoothness of the slip distribution, we construct a Bayesian model with unknown hyperparameters and draw samples from the posterior PDF regarding the SDR distribution. The method implemented herein is adopted from Yabuki & Matsu'ura (1992), which determined the hyperparameters using an information criterion instead of performing Bayesian sampling (see the Appendix for details).

Fig. 5(b) shows the estimated PDF using the conventional approach with $\theta = 18^\circ$ (the standard deviation of θ is not discussed because the uncertainty of the parameter on the underground structure cannot be introduced in the conventional approach). The true values in some of the

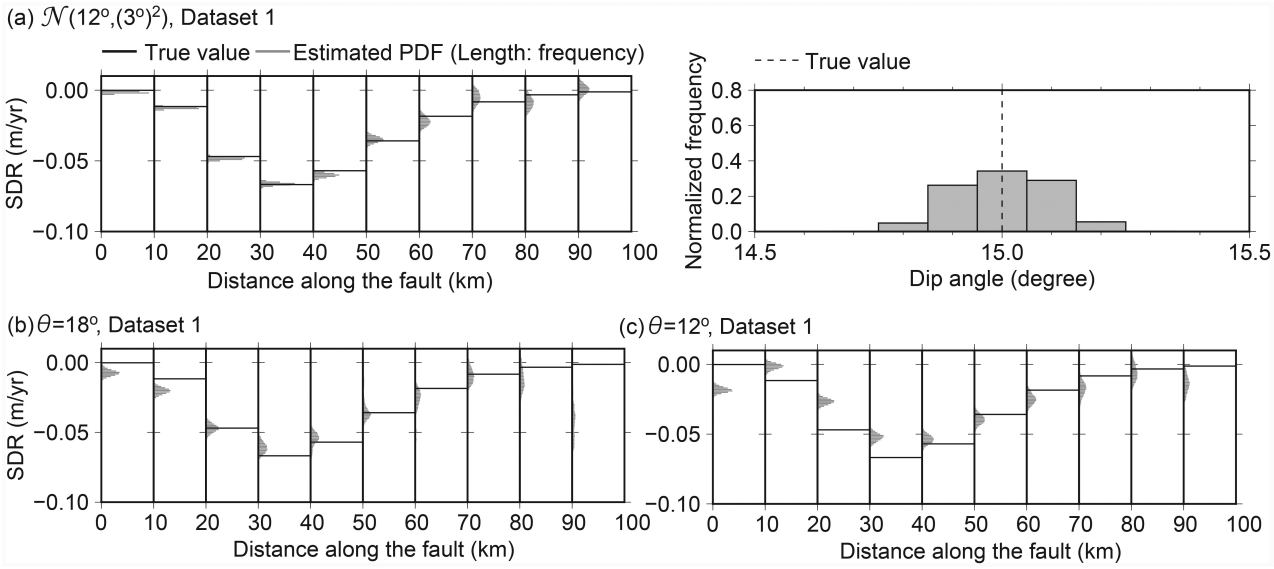

Figure 5. The estimation result based on a different assumption of the mean value of the dip angle and comparison with a conventional approach based on a smoothing constraint. (a) The estimation result of SDR and the dip angle in a case using Dataset 1 and assuming that θ follows $\mathcal{N}(12^\circ, (3^\circ)^2)$. (b) The estimation result of SDR using a conventional approach based on a smoothing constraint and assuming $\theta = 18^\circ$. (c) The estimation result of SDR using a conventional approach based on a smoothing constraint and assuming $\theta = 12^\circ$.

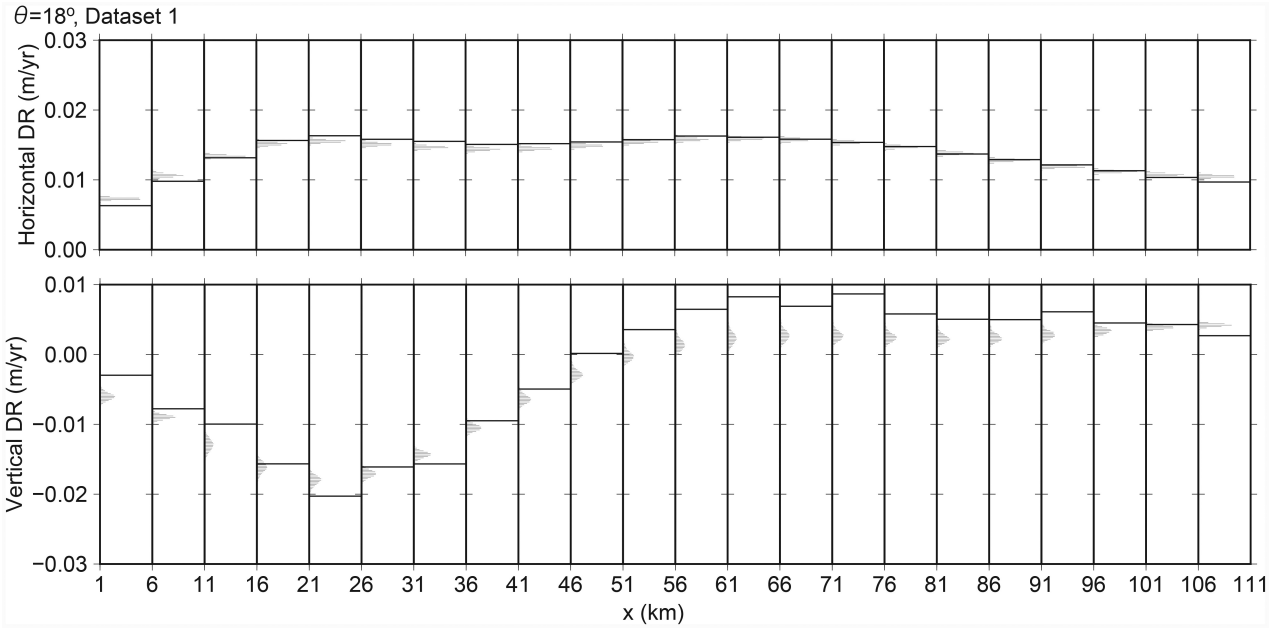

Figure 6. The posterior predicted PDF of horizontal and vertical displacement rate (DR) using a conventional approach based on a smoothing constraint and assuming $\theta = 18^\circ$.

small faults are quite distant from the main part of the histograms, particularly in the shallowest and deepest edges of the fault. Fig. 6 shows that the predicted distribution explains well the horizontal component of the data, which is associated with smaller errors. However, the model poorly explains the vertical component, that is, overfitting the data in the horizontal component occurs because important characteristics of the noise, such as covariance components in the prediction errors (e.g. Yagi & Fukahata 2008, 2011), are missing in the formulation. This situation results in the estimation of the posterior PDF that is statistically inconsistent with the true model parameters. Fig. 5(c) shows the same estimation with a different assumption for the dip angle, $\theta = 12^\circ$. The histograms appear different from the true values and those obtained with $\theta = 18^\circ$. In cases where a significant amount of prediction errors is included in the prediction model, a conventional approach that does not distinguish the prediction errors from observation errors can produce estimation results that are highly dependent on the model assumptions, which is contrary to the results obtained using the proposed method. These findings are consistent with the arguments made by Minson *et al.* (2013) and Duputel *et al.* (2014) on the discrepancy in the published fault slip models for the same earthquake, which we mention in Section 1.

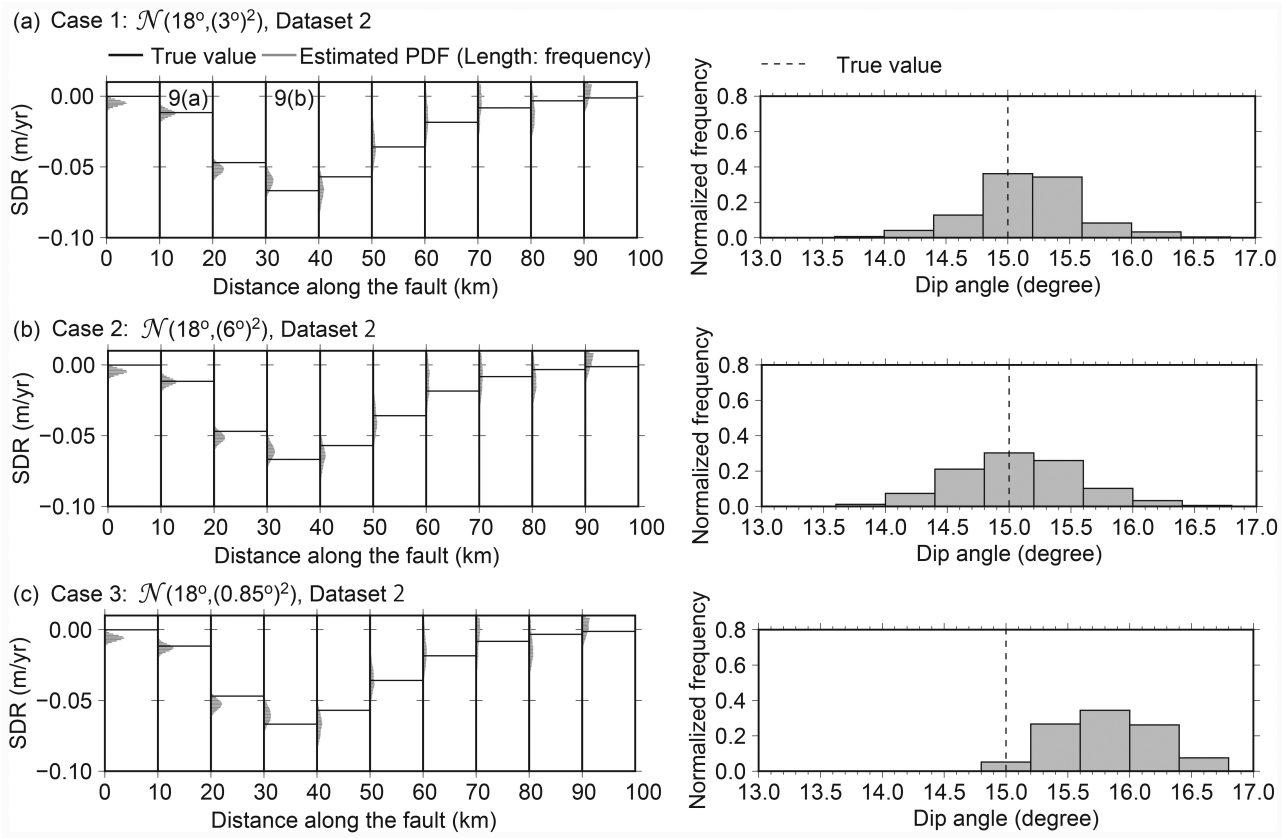

Figure 7. Comparison of the estimation results in Cases 1, 2 and 3. (a) The estimation result of the posterior PDF of SDR and the dip angle in Case 1, using Dataset 2 and assuming that θ follows $\mathcal{N}(18^\circ, (3^\circ)^2)$. The marks 9(a) and 9(b) have been mentioned in Fig. 9. (b) The estimation result of the posterior PDF of SDR and the dip angle in Case 2, assuming that θ follows $\mathcal{N}(18^\circ, (6^\circ)^2)$. (c) The estimation result of the posterior PDF of SDR and the dip angle in Case 3, assuming that θ follows $\mathcal{N}(18^\circ, (0.85^\circ)^2)$.

4.2.2 Variation of the solution versus different assumptions on the uncertainty of the underground structure

The results in Section 4.2.1 suggest that the proposed method can produce estimation results that are less dependent on an assumption of the mean value of the underground structure parameter as long as the variance is set properly. Next, we examine the importance of the variance, or, more generally, the uncertainty, of the underground stucture parameter in the estimation. To show the impact of changing the variance on the estimation results more clearly, we use Dataset 2, in which the accuracy of synthetic DR data for the horizontal component is one-order lower than that of Dataset 1. We consider three cases where the dip angle follows $\mathcal{N}(18^\circ, (3^\circ)^2)$, $\mathcal{N}(18^\circ, (6^\circ)^2)$ and $\mathcal{N}(18^\circ, (0.85^\circ)^2)$, which we refer to as Cases 1, 2, and 3, respectively.

Fig. 7(a) shows the results in Case 1, where θ follows $\mathcal{N}(18^\circ, (3^\circ)^2)$. Because the data are less accurate, the uncertainty in the estimation results of both the SDR and dip angle becomes larger than that in the base case. In addition, we observe that the shape of the histogram is slightly biased from the true value for the mean value of the prior PDF, 18°. Because of the large uncertainty that we assume for the observation errors, more emphasis is placed on the prior dip angle information than in the base case. In the posterior prediction distribution (Fig. 8), gentler function shapes than those with Dataset 1 are drawn in the horizontal components, which also reflects the larger variance for the observation errors.

The estimated PDFs in Case 2 (Fig. 7b), where θ follows $\mathcal{N}(18^\circ, (6^\circ)^2)$, also have the same characteristics as the result obtained in Case 1, in that, the histogram for the estimated dip angle appears similar. However, the histogram for Case 2 is less biased for the mean value of the dip angle. Fig. 9 shows close-up views of the samples of the posterior PDF for SDR and the posterior prediction PDF as examples. The drawn curves for Case 2 look almost identical to those for Case 1. After additional trials, we found that the basic characteristics remain the same even when a larger σ is adopted for the PDF of the dip angle. This finding can be understood as follows. As the variance of the dip angle increases, the likelihood of the true value $\theta = 15^\circ$ for the assumed PDF of the dip angle increases as well. For example, the true value $\theta = 15^\circ$ corresponds to the $1/2\sigma$ value for $\mathcal{N}(18^\circ, (6^\circ)^2)$, while corresponding to 1σ for $\mathcal{N}(18^\circ, (3^\circ)^2)$, the true value $\theta = 15^\circ$ becomes a more likely realization as the variance becomes larger in the assumed PDF. From another viewpoint, when large uncertainty on the prior information of the underground structure parameter is assumed, more emphasis is placed on the observation data. Thus, the results almost exclusively reflect the information obtained from the observation data.

In Case 3, we estimated the posterior PDF of SDR assuming that θ follows $\mathcal{N}(18^\circ, (0.85^\circ)^2)$, in which the true value $\theta = 15^\circ$ corresponds to approximately 3.5σ (Fig. 7c). For this PDF, the true dip angle corresponds to an unlikely realization. Such a setting results in requirement

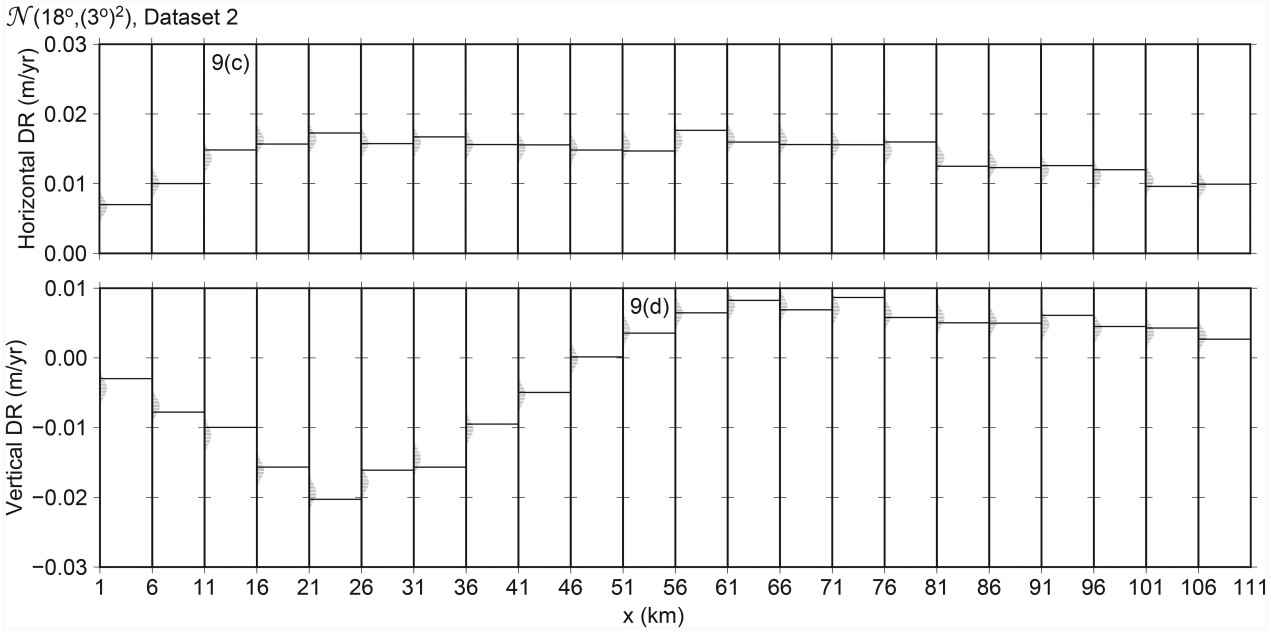

Figure 8. The posterior predicted PDF of horizontal and vertical displacement rate (DR) for Case 1. The marks 9(c) and 9(d) have been mentioned in Fig. 9.

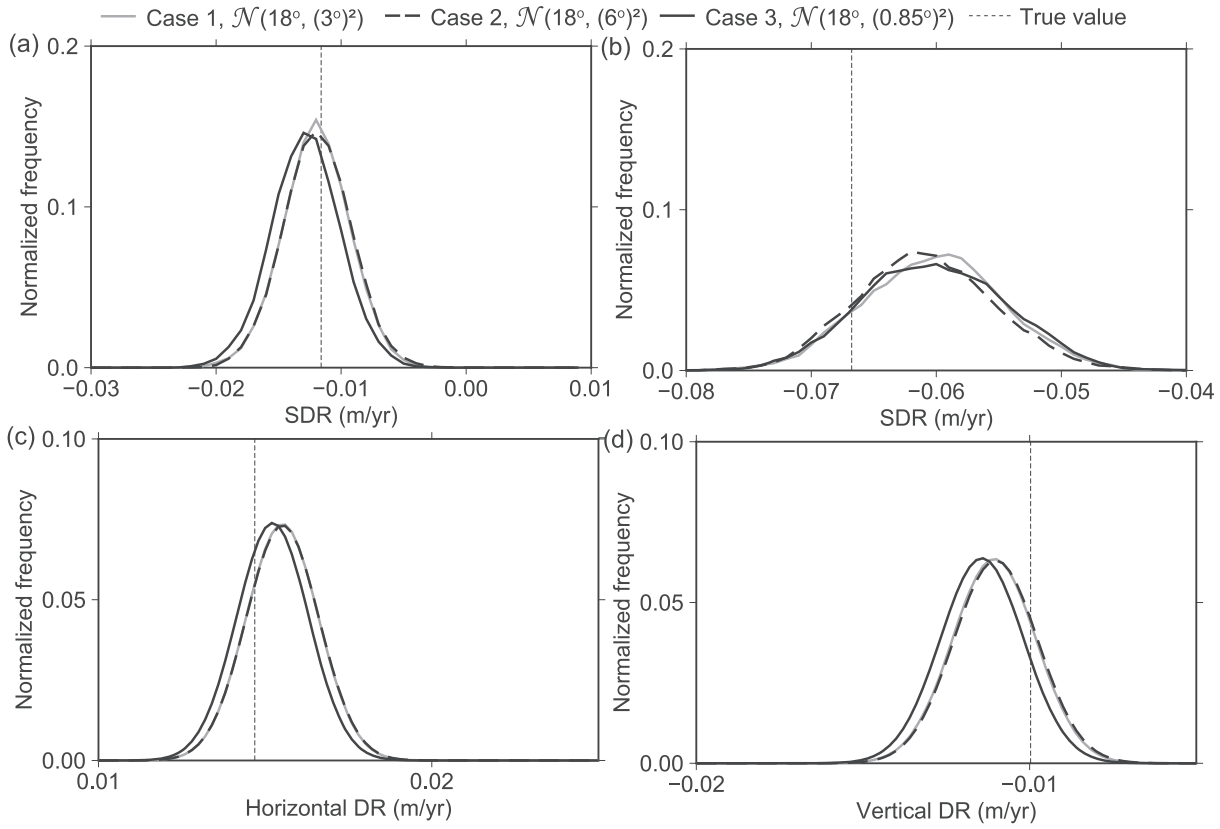

Figure 9. Close-up views of the samples of the posterior PDF for SDR and the posterior prediction PDF of Cases 1, 2 and 3. (a and b) Comparison of the posterior PDFs in the fault patches 9(a) and 9(b) marked in Fig. 7. (c and d) Comparison of the posterior prediction PDFs in the observation points 9(c) and 9(d) marked in Fig. 8.

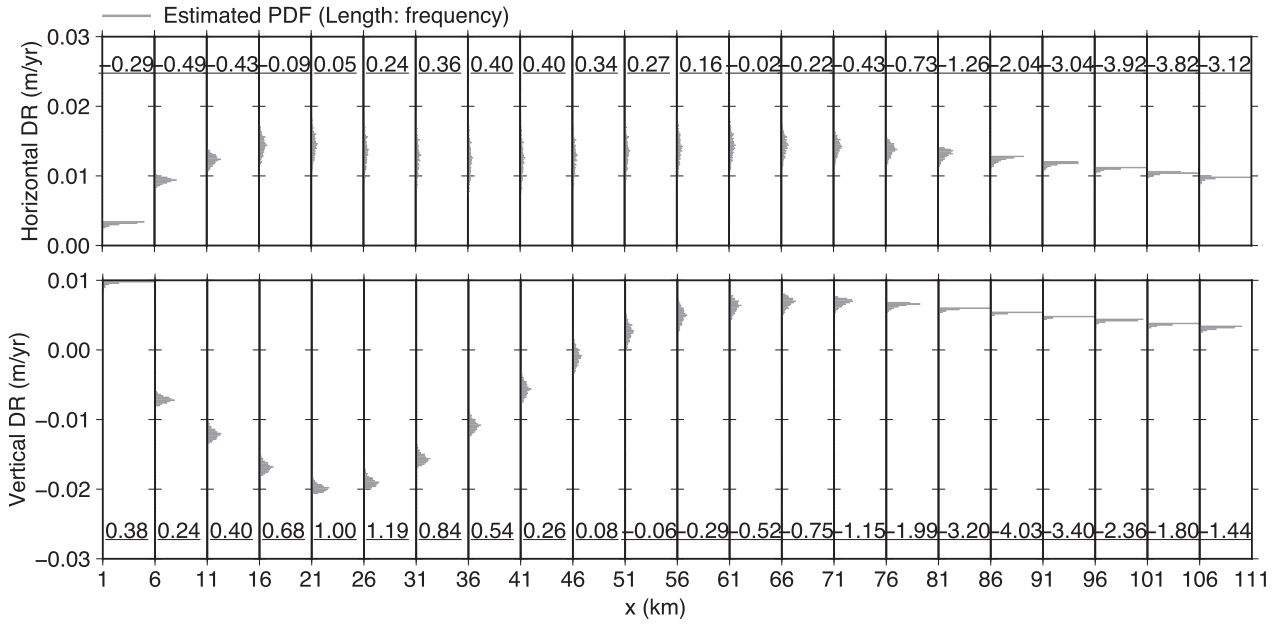

Figure 10. The PDF for prediction errors associated with the mean of the sampled model parameters $\bar{\mathbf{m}}$ in the base case. The underlined numbers are the skewness of the PDF of the model parameter evaluated at each surface observation point.

of a larger ensemble size, in this case $N = 10\,000$, to obtain a converged PDF (see Section 4.2.4 for a detailed discussion). In the right-hand panel, we observe that the peak of the histogram is located near the bin of 16°, from which we see a significant impact from the mean value in the prior PDF. It follows that a larger weight is placed on the prior information of the dip angle in this case because of its relatively small uncertainty. The estimated SDR distributions in the left-hand panel appear similar to those in Cases 1 and 2. However, the close-up views of the samples of the posterior PDF for SDR and the posterior prediction PDF (Fig. 9) reveal small but significant differences between the results in Case 3 and those in the two other cases for certain fault patches and observation points. Notably, the three cases estimate similar function shapes for a fault patch located at a deeper portion of the fault plane (Fig. 9b), probably because the surface DR response to fault slip in a deeper portion is less sensitive to the change in the dip angles. Moreover, the estimates of Cases 1 and 2 are not always closer to the true values than those of Case 3 (e.g. Fig. 9c) because of the randomness of the artificial noise included in the synthetic data.

In summary, the uncertainty of the underground structure has an impact on the estimation results by determining the balance between the observation data and the prior information on the underground structure. In our problem setting, as the variance of the dip angle increases, more emphasis is placed on the information in the data. As a result, the estimation result does not strongly depend on the variance of the dip angle if the variance changes in a range of values that are large to some extent. As the variance of the dip angle decreases, more emphasis is placed on the prior information. In such a situation, if the mean value of the prior PDF for the dip angle is significantly different from the true one, the estimation results of the SDR, dip angle, and posterior prediction of DR are less consistent with the true values. Such a tendency for the impact of uncertainty is easily highlighted herein because our toy problem exclusively adopts one parameter for the underground structure, and the data are sufficiently sensitive to changes in the dip angle. In common with the usual manner of Bayesian inference, inaccurate prior information on parameters that are sensitive to the data significantly contaminate the inversion result. More complicated situations expected in real-world problems are discussed in Section 5.

4.2.3 Non-Gaussianity of the prediction errors

One advantage of the proposed method over previous studies is that the assumption of Gaussian distribution on the prediction errors is not necessary, because the integration to associate the prediction and observation errors shown in eq. (2) is performed based on Monte Carlo integration. We plot an example set of the PDF for prediction errors evaluated at the surface observation points, which is identical to the second term of the integrand in eq. (2), that is, $P(\mathbf{d}_{\rm pred}|\mathbf{m})$, in Fig. 10 for the base case. Because the PDF for prediction errors depends on the choice of $\mathbf{m}$, we choose $\bar{\mathbf{m}}$ as a representative case and adopt $P(\mathbf{d}_{\rm pred}|\bar{\mathbf{m}})$ for plotting, where $\bar{\mathbf{m}} = \frac{1}{M}\sum_{m=1}^{M}\mathbf{m}^{(m)}$ is the mean of the samples from the posterior PDF. We observe shapes for the distribution that are significantly different from the Gaussian distribution at some observation points. The underlined numbers in the figure are the skewness, which is a statistic that can be used as a metric of the discrepancy of the target PDF from the Gaussian distribution of the estimated prediction errors at each observation point. A widely known rule of thumb for interpreting the skewness (Bulmer 1979) is:

(1) A distribution with a skewness less than -1 or greater than $+1$ is highly skewed.

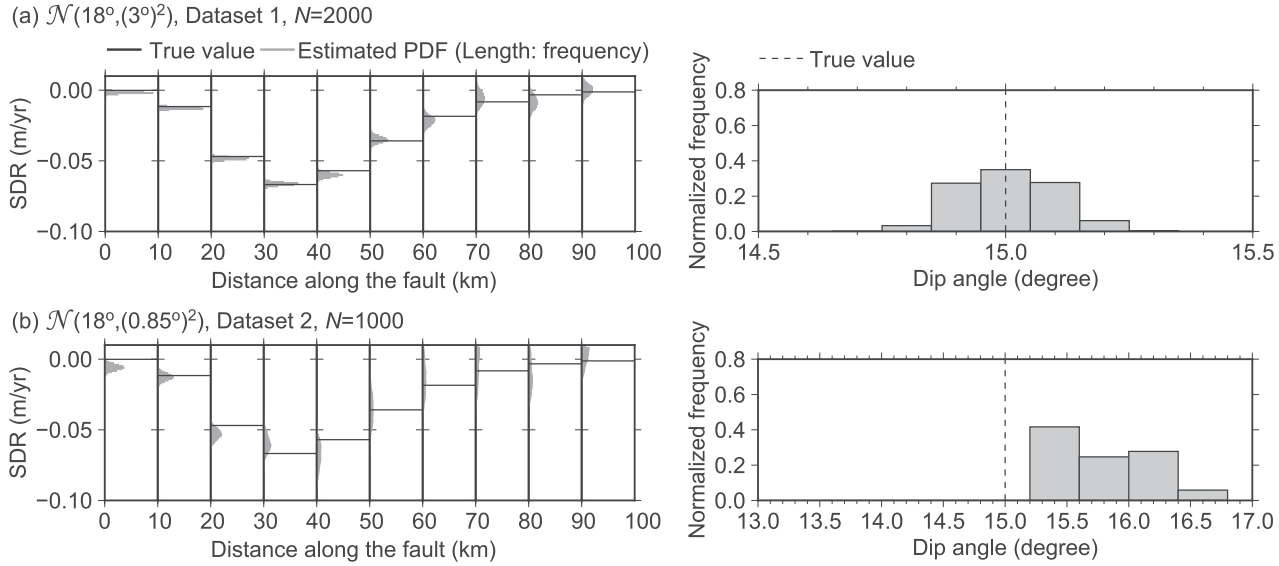

Figure 11. The estimation results with the ensemble sizes. (a) The estimation result of the posterior PDF of SDR and the dip angle with the ensemble size 2000 for the same setting as the base case. (b) The estimation result of the posterior PDF of SDR and the dip angle with the ensemble size 1000 for the same setting as Case 3.

(2) A distribution with a skewness between -1 and -0.5 or between $+0.5$ and $+1$ is moderately skewed.
(3) A distribution with a skewness between -0.5 and $+0.5$ is approximately symmetric.

The estimated PDF in more than one-third of the observation points in Fig. 10 is considered to be a highly skewed distribution, for which the Gaussian approximation might not be appropriate. These findings indicate that the assumption of Gaussian distribution of the prediction errors may introduce some bias in the estimation of the posterior PDF.

4.2.4 Ensemble size to model the uncertainty of Green's functions

In most analyses presented above, we employed $N = 1000$ for the samples of the dip angle drawn from a PDF that represents its stochastic property. We examined whether the number of samples is enough for estimating the posterior PDF. Figs 11(a) and (b) show the estimation result using 2000 samples in the same setting as that of the base case. Little change is observed from the result obtained using 1000 samples in the estimated PDF for the slip parameters. The posterior PDF for the dip angle estimated with $N = 2\,000$ shows good agreement with the result in the base case with $N = 1000$, in that, most of the samples with weight fall within $\theta = 14.85^\circ$ and 15.15°. However, the case with $N = 2000$ has a taller peak in the central bin. The histogram for the posterior PDF of the underground structure parameter appears to be more sensitive to the ensemble size because the number of samples of the underground structure parameter is identical to the number of items to draw the histogram. These findings indicate that $N = 1000$ is sufficient for estimating the posterior PDFs; however, a more detailed investigation of that for the underground structure parameter may require a larger ensemble size. Such a feature is evident in the setting of Case 3 in Section 4.2.2, which can be attributed to a small variance in the assumed PDF for the dip angle. Figs 11(c) and (d) show the results obtained with $N = 1000$ of the dip angle for the same setting as Case 3. The histogram for the posterior PDF of the dip angle is unnaturally truncated in the boundary of the bins between 15° and 15.5°, although the result for SDR looks quite consistent with other results. This result is understandable because the true value $\theta = 15^\circ$ corresponds to 3.5σ in this distribution, meaning that the probability of a sample of θ being smaller than 15° is drawn is approximately 2.3×10^{-4}. One thousand samples are not sufficient to approximate the shape of the PDF around 15°. The result presented in Section 4.2.2 required $N = 10\,000$ to show a converged solution. In such a case, the assumed PDF for the underground structure parameters should be revised rather than further increasing the ensemble size to obtain a converged solution (see Section 5.4 for a detailed discussion). From this result, we conclude that the ensemble size sufficient to approximate the posterior PDF of the model parameters depends on the assumed PDF for the underground structure parameters.

The number of samples for the REMC exploration $M_{\text{iteration}} = 500\,000$ is a sufficiently large number to obtain a converged solution in all the cases presented in this study. It should be noted that this section presents an example using only one underground structure parameter. The case with multiple underground structure parameters is discussed in Section 5.4.

5 DISCUSSION OF APPLICATIONS TO REAL-WORLD PROBLEMS

The application example of the proposed method to a simple problem presented in the previous section demonstrates the basic aspects of the method. Based on these findings, we discuss the application of the proposed method to real-world problems in this section.

5.1 Regularization-free slip inversion

In the previous section, we compared the estimation results obtained using the proposed method and a method based on the regularization of smoothing constraints. With an aim to discuss the results in terms of real-world applications, we first summarize the role of the regularization based on prior constraints, including that based on the smoothing constraint, in a typical slip inversion method. Regularization based on prior constraints is known to help inversion analyses in two aspects:

(1) the inverse problems in the real world are often ill-posed (in majority of such cases, non-uniqueness of the solution is not satisfied). In the worst case, the coefficient matrix is not numerically invertible. The introduction of regularization enables us to solve such inverse problems by eliminating tiny singular values of the coefficient matrix.

(2) Even if the problem is numerically solvable, the estimation result may overfit the noise originating from the observation and model prediction errors due to the ill-conditioned nature of the problem. By balancing the information from the data and the penalty introduced by the regularization based on the physical or empirical prior knowledge, overfitting the noise is reduced.

However, as Yagi & Fukahata (2008, 2011) pointed out, even if a proper regularization is applied, missing important noise characteristics in the inversion scheme, such as covariance components in the prediction errors, possibly still induces overfitting and distorts the estimated slip distribution. These issues may be the reasons for the significant discrepancy of available fault slip models for the same earthquake, with which it is not easy to draw a meaningful conclusion about the source process (Minson *et al.* 2013; Duputel *et al.* 2014). Furthermore, it is generally difficult to find a regularization method that has strong scientific evidence for the slip inversion. However, the choice of the regularization method often largely changes the estimation result of slip distribution. For example, the introduction of a type of sparsity-promoting constraint to an estimation of slip distribution in long-term slow slip events in the Nankai Trough region in south-west Japan resulted in significantly different up- and down-dip limits for slip distribution from those obtained using smoothness constraints (Nakata *et al.* 2017). More sophisticated implicit (e.g. trans-dimensional inversion Dettmer *et al.* 2014) and explicit (e.g. von Karman regularization Amey *et al.* 2018, 2019) regularization schemes have been introduced to fault slip estimations, and it is reported that these methods significantly outperformed the traditional method based on smoothing constraint in flexibility.

The combination of Bayesian inference and mathematically rigorous treatment of the observation and prediction errors, such as presented in this study, can be an alternative solution to ill-posedness and overfitting in the slip inverse problems: Ill-posedness of the inverse problem does not become severe in the framework of Bayesian inference, because the computation of matrix inverse is not required: The non-uniqueness of the solution results in a nearly uniform posterior PDF of the target parameter. Overfitting due to the ill-conditioned system can be avoided by accurately handling the stochastic properties of the errors in the target posterior PDF. Previous studies such as Duputel *et al.* (2014), Ragon *et al.* (2018) and Gombert *et al.* (2018) performed slip inferences without regularization based on such an idea. We expect that the proposed method has the potential to be a powerful tool to perform slip inversions that are free from the choice of the regularization method for a given structured grid that discretizes the fault plane. However, it should be noted that the choice of the grid size and basis functions to parametrize the slip distribution can implicitly control its smoothness, too. Notably, we did not discuss the resolution power in the estimations presented in Section 4, because we applied only single patterns of fault discretization, based on which synthetic data are also calculated. The issue of the choice of the grid size and basis functions when the proposed method is used as a regularization-free slip estimation method (Minson *et al.* 2013; Duputel *et al.* 2014) needs further consideration. It should be also noted that the proposed method can be used combined straightforwardly with a proper regularization method chosen from the previously proposed ones (e.g. Yabuki & Matsu'ura 1992; Dettmer *et al.* 2014; Nakata *et al.* 2017; Amey *et al.* 2018, 2019), because of the flexibility of the Bayesian sampling method.

5.2 PDF for the underground structure parameters and the ensemble size N

In the application of the proposed method for earthquake source estimations using geodetic or seismic waveform data, we first need to set an underground structure model associated with its uncertainty information. An ideal situation is that the seismic velocity structure and the fault geometry associated with their uncertainty information are provided as a database based on seismic exploration, seismicity analysis, and other estimation methods. If the information is prepared in the form of an ensemble of the possible underground structure models, the proposed method can directly import the ensemble to calculate that of Green's functions. For instance, MCMC samples of 1-D velocity structure jointly estimated with local hypocentres (Ryberg & Haberland 2019) can be directly imported to a source estimation based on 1-D velocity structure using the proposed method. Estimation of 3-D underground structure based on MCMC typically required a larger number of the samples (e.g. Bodin & Sambridge 2009; Bodin *et al.* 2012; Hawkins & Sambridge 2015; Piana Agostinetti *et al.* 2015), with which direct importing of the samples to the proposed method may become difficult in terms of computation cost. However, combination of those approach with advanced sampling algorithms, such as the Hamiltonian Monte Carlo method (e.g. Fichtner *et al.* 2019; Gebraad *et al.* 2020), may results in a smaller number of samples to approximate the posterior, with which the proposed method is applicable. Currently, because most of the available databases on the seismic velocity structure and fault geometry (e.g. Koketsu *et al.* 2012; Laske *et al.* 2013) are not associated with the estimation errors, we usually need to set the prior PDFs of $\boldsymbol{\varphi}$ that describe the stochastic property of the underground structure in an ad-hoc manner. A possible practice is to compare multiple different databases and information for the target underground structure and assume values of the mean and variance of Gaussian distribution for each parameter. In some situations where there is little information that

can be used to assume the PDFs, a method based on Gaussian approximation of the error property with an empirical choice of a non-diagonal covariance matrix (e.g. Dettmer *et al.* 2007; Yagi & Fukahata 2008, 2011; Agata 2020) may outperform the proposed method.

The proposed method can update the information on the underground structure via earthquake source estimation using seismic waveforms, geodetic data, and/or other kinds of observation data regarding earthquakes. When a new event is analysed following an analysis of a previous event in the same region, a new underground structure model that was updated via the previous analysis can be used. Such an update of the underground structure parameters can be interpreted as 'update of the model class' in the context of Bayesian framework as discussed in Beck (2010) and Minson *et al.* (2014).

The results shown in Section 4.2.4 indicate that unboundedness of the assumed PDF sometimes leads to a demand for an enormous ensemble size N to obtain a converged posterior PDF. Based on our knowledge of nature, it is usually reasonable to consider the range of underground structure parameters as bounded rather than unbounded. In such a case, the use of a PDF that is bounded on one side or both, such as the Gamma distribution or the truncated normal distribution, by making use of the flexibility of the ensemble-based method in terms of choice of PDFs, may be more appropriate than using an unbounded distribution such as the Gaussian distribution. The discussion in Section 4.2.4 additionally suggests that the difficulty in obtaining a converged posterior PDF indicates an inconsistency between the assumed PDF of the underground structure parameters and the real underground structure because such difficulty may have originated from a low likelihood of the true value for the assumed PDF.

5.3 PDF for the underground structure parameters and the estimation results

We discuss the impact of the prior information of a underground structure parameter on the estimation results. We first focus on the impact on the estimation results of the model and the underground structure parameters. As seen in Section 4.2.2, the estimation results almost directly reflects the information in the observation data if we set a large uncertainty for the underground structure parameter. If the uncertainty for the underground structure parameter is small and a significant amount of bias from the true value is included in the prior information, the estimation results of the model and underground structure parameter also include bias. The examples in Section 4.2.2 present only a small bias in the results, but it is only because of the small bias in the prior information for the underground structure parameter.

Further, we discuss the impact of the prior information on a underground structure parameter on the prediction. If the data contains sufficient information on the underground structure parameter, a bias in the prior information on the underground structure parameter results in a bias in the posterior prediction PDF, as well as in the estimation of the model and the underground structure parameters. On the other hand, predicting the response at a point in the space and time where the data does not exist is sometimes fundamentally important. Even if the data do not contain enough information on a underground structure parameter, accurate information on the underground structure parameter with small bias and low uncertainty can be a key factor in carrying out accurate predictions. The meaning of 'prediction' herein is not limited to the calculated response based on the estimated slip distribution, but also applies to the prediction of events in the future, for example, prediction of post-earthquake deformation based on an estimated co-seismic slip model (Iinuma 2018) and dynamic rupture scenario of an earthquake based on an estimation of SDRs in interseismic periods (Hok *et al.* 2011).

Notably, the proper parametrization of the underground structure, such as decomposition of the structure into stratified layers and choice of controlling parameters of the fault geometry, essentially requires knowledge of the structure.

5.4 Multiple underground structure parameters and the ensemble size N

In applying the proposed method to real-world problems, we need to introduce at least several underground structure parameters to parametrize the stochastic properties of the target underground structure. In future work, we need a more general discussion about the ensemble size N for such a case, because consideration of a high-dimensional parameter space may cause a severe problem in terms of computation cost due to requirement of a large ensemble size, which can be considered as a type of 'the curse of dimensionality' (Bellman 1957).

Estimation the posterior PDF of $\boldsymbol{\varphi}$ may suffer from explosion of the ensemble size in such a case because the number of the underground structure parameters is identical to the dimension of the PDF. On the other hand, Provided that we focus on the estimation of the model parameters, the practice of using the Ensemble Kalman Filter (EnKF) is encouraging: EnKF usually uses a modest ensemble size (i.e. of the order of 10^2) to approximate the stochastic property of the errors of the data vector in a typical meteorological problem. This ensemble size is used because the response in the observation space is spatially localized due to the nature of the governing equation. In the problems of seismology, this should also be the case, at least, for the slip estimations using geodetic data, because the elastic deformation, which rapidly decays with distance, is the basic physics for the problems. In the estimations using seismic waveform data, we may need a larger ensemble size than in the geodetic estimations in some problem settings, because the Green's function is less localized spatially in the wave equation. Further study may be required to overcome the potentially larger computation cost associated with the application of the proposed method to such problems.

5.5 Other components of model prediction errors

The scope of study is restricted to an assumption that the major component of the model prediction errors is due to the uncertainty of the underground structure. However, effects from other components of model prediction errors, such as those due to the choice of the governing partial differential equation, discretization errors and so on, can also be significant for the estimation results in some cases. Some of such components can be introduced by designing a non-diagonal $\mathbf{E}$ (e.g. the approach of Yagi & Fukahata (2008) for the discretization errors) and adding to the data covariance matrix $\mathbf{E}$ in eq. (5). If the contribution of such components is expected to be relatively small, the use of a covariance matrix with the form of $\sigma^2\mathbf{E}$, where $\mathbf{E}$ is a simple diagonal matrix and the scaling factor σ^2 is estimated via a hierarchical Bayesian framework (e.g. Yabuki & Matsu'ura 1992), might work properly. However, further studies are required for proposing a comprehensive modelling framework that can also consider other components of model prediction errors more accurately.

6 CONCLUSIONS

We developed a flexible Bayesian inference method for estimating fault slips that can accurately incorporate non-Gaussian prediction errors, considering the uncertainty of the underground structure based on ensemble modelling. The flexibility of the probability distribution shape is maintained by performing the integration for evaluating the likelihood function based on the Monte Carlo approximation using the samples in the ensemble of Green's functions, instead of assuming a Gaussian distribution that allows for analytically evaluating the integration. The framework can additionally estimate the posterior PDF of the parameters of the underground structure by evaluating the likelihood of each sample in the ensemble through the Bayesian sampling.

To validate the advantage of the proposed method, we performed simple numerical experiments for estimating SDR distributions on a thrust fault in a 2-D elastic half-space using synthetic data of surface displacement rates, in which the dip angle of the fault plane is the parameter used to characterize the underground structure. In a scenario wherein the information on the dip angle is uncertain and inaccurate, the proposed method succeeded in estimating posterior PDFs of SDR that are consistent with the true SDR, even for different mean values of the prior Gaussian PDF. Furthermore, this method could estimate a posterior PDF of the dip angle that has a strong peak around the true value. With equivalently inaccurate dip angles, the results obtained using a conventional approach, which does not explicitly distinguish the prediction and observation errors and introduces regularization based on smoothing constraints, included a significant amount of bias, which was not witnessed in the experiments using the proposed method. We also applied different values of the variance of the prior PDF for the dip angle and examined the impact on the estimation results. As a result, once the variance of the dip angle becomes large to some extent, we observe low dependence of the estimation result on the value of the variance. In contrast, as the variance of the dip angle becomes smaller, more emphasis was put on the prior information. In such a case, when the mean value of the prior PDF of the dip angle was significantly different from the true one, the estimation results of the dip angle was significantly biased for the mean value. As a result, the estimation of the posterior PDF of SDR and the posterior prediction of DR also included a significant amount of bias from those estimated based on a larger variance in the prior PDF of the dip angle. Moreover, the prior PDF of the dip angle that was inconsistent with the true value (i.e. the likelihood of the true value for the prior PDF is very small) required a significantly larger ensemble size to obtain convergence of the posterior PDF. The distribution shapes of the prediction errors for the representative model parameters in some observation points were quite asymmetric, with the absolute value of the sample skewness larger than one, for which Gaussian approximation is not usually applied. This result indicates that the flexibility of the probability distribution shape due to the application of ensemble-based modelling may contribute to the high accuracy of the analyses.

We further discussed the important points to consider in applying the proposed method to real-world problems. We suggested that the proposed method can be a candidate as a powerful tool for regularization-free slip inversions because our Bayesian sampling algorithm that accurately handles Non-Gaussian prediction errors can provide an alternative solution to the ill-posedness and ill-conditioning of the inverse problems. Based on the speculation that the spatial locality of the response due to the nature of the governing equation reduces the ensemble size that is necessary to model the uncertainty of underground structure, geodetic slip inversions using elastic deformation models, in which the response decays rapidly with distance, are expected to be a relatively easier problem to take on. On the contrary, in the problems using the seismic waveform data, such as waveform slip inversions and hypocentre determinations, simultaneous estimation of the source and the underground structure should become more interesting topic because the data consist of waves from many paths and are expected to include more information of the underground structure. In return, more computation efforts may be required to deal with a large amount of computation cost due to the large ensemble size.

ACKNOWLEDGEMENTS

We thank Dr Sarah Minson and Dr Jan Dettmer for their insightful and constructive review comments. We appreciate the comments on Bayesian sampling methods by Dr Hiromichi Nagao and Dr Shin-ichi Ito. This research was supported by JSPS KAKENHI Grant Number JP19H04631 in Scientific Research on Innovative Areas 'Science of Slow Earthquakes'. Some figures were produced using GMT software (Smith & Wessel 1990).

REFERENCES

Agata, R., 2020. Introduction of covariance components in slip inversion of geodetic data following a non-uniform spatial distribution and application to slip deficit rate estimation in the Nankai Trough subduction zone, *Geophys. J. Int.,* **221**(3), 1832–1844.

Agata, R., Ichimura, T., Hori, T., Hirahara, K., Hashimoto, C. & Hori, M., 2018. An adjoint-based simultaneous estimation method of the asthenosphere's viscosity and afterslip using a fast and scalable finite-element adjoint solver, *Geophys. J. Int.,* **213**(1), 461–474.

Amey, R., Hooper, A. & Walters, R., 2018. A Bayesian method for incorporating self-similarity into earthquake slip inversions, *J. geophys. Res.,* **123**(7), 6052–6071.

Amey, R., Hooper, A. & Morishita, Y., 2019. Going to any lengths: solving for fault size and fractal slip for the 2016, M_w 6.2 Central Tottori earthquake, Japan, using a transdimensional inversion scheme, *J. geophys. Res.,* **124**(4), 4001–4016.

Beck, J.L., 2010. Bayesian system identification based on probability logic, *Struct. Control Health Monit.,* **17**(7), 825–847.

Bellman, R., 1957. *Dynamic Programming,* Dover Publications.

Bishop, C.M., 2006. *Pattern Recognition and Machine Learning,* Springer.

Bodin, T. & Sambridge, M., 2009. Seismic tomography with the reversible jump algorithm, *Geophys. J. Int.,* **178**(3), 1411–1436.

Bodin, T., Sambridge, M., Rawlinson, N. & Arroucau, P., 2012. Transdimensional tomography with unknown data noise, *Geophys. J. Int.,* **189**(3), 1536–1556.

Bulmer, M.G., 1979. *Principles of Statistics,* Courier Corporation.

Dettmer, J., Dosso, S.E. & Holland, C.W., 2007. Uncertainty estimation in seismo-acoustic reflection travel time inversion, *The J. acoust. Soc. Am.,* **122**(1), 161–176.

Dettmer, J., Benavente, R., Cummins, P.R. & Sambridge, M., 2014. Transdimensional finite-fault inversion, *Geophys. J. Int.,* **199**(2), 735–751.

Duputel, Z., Agram, P.S., Simons, M., Minson, S.E. & Beck, J.L., 2014. Accounting for prediction uncertainty when inferring subsurface fault slip, *Geophys. J. Int.,* **197**(1), 464–482.

Evensen, G., 1994. Sequential data assimilation with a nonlinear quasi-geostrophic model using Monte Carlo methods to forecast error statistics, *J. geophys. Res.,* **99**(C5), 10 143–10 162.

Fichtner, A., Zunino, A. & Gebraad, L., 2019. Hamiltonian Monte Carlo solution of tomographic inverse problems, *Geophys. J. Int.,* **216**(2), 1344–1363.

Fukahata, Y. & Wright, T.J., 2008. A non-linear geodetic data inversion using ABIC for slip distribution on a fault with an unknown dip angle, *Geophys. J. Int.,* **173**(2), 353–364.

Fukuda, J. & Johnson, K.M., 2008. A fully Bayesian inversion for spatial distribution of fault slip with objective smoothing, *Bull. seism. Soc. Am.,* **98**(3), 1128–1146.

Fukuda, J. & Johnson, K.M., 2010. Mixed linear–non-linear inversion of crustal deformation data: Bayesian inference of model, weighting and regularization parameters, *Geophys. J. Int.,* **181**(3), 1441–1458.

Gebraad, L., Boehm, C. & Fichtner, A., 2020. Bayesian elastic full-waveform inversion using Hamiltonian Monte Carlo, *J. geophys. Res.,* **125**(3), e2019JB018428, doi:10.1029/2019JB018428.

Geyer, C.J., 1991. *Markov Chain Monte Carlo Maximum Likelihood,* Interface Foundation of North America.

Gombert, B., Duputel, Z., Jolivet, R., Simons, M., Jiang, J., Liang, C., Fielding, E.J. & Rivera, L., 2018. Strain budget of the Ecuador–Colombia subduction zone: a stochastic view, *Earth planet. Sci. Lett.,* **498,** 288–299.

Gordon, N.J., Salmond, D.J. & Smith, A.F., 1993. Novel approach to nonlinear/non-Gaussian Bayesian state estimation, *IEE Proc. F,* **140,** 107–113.

Hallo, M. & Gallovič, F., 2016. Fast and cheap approximation of green function uncertainty for waveform-based earthquake source inversions, *Geophys. J. Int.,* **207**(2), 1012–1029.

Hawkins, R. & Sambridge, M., 2015. Geophysical imaging using trans-dimensional trees, *Geophys. J. Int.,* **203**(2), 972–1000.

Hok, S., Fukuyama, E. & Hashimoto, C., 2011. Dynamic rupture scenarios of anticipated Nankai–Tonankai earthquakes, southwest Japan, *J. geophys. Res.,* **116**(B12), doi:10.1029/2011JB008492.

Iinuma, T., 2018. Postseismic uplift along the Pacific coast of Tohoku and Kanto districts associated with the 2011 off the Pacific coast of Tohoku earthquake, *J. Disaster Res.,* **13**(3), 496–502.

Iinuma, T., Hino, R., Kido, M., Ohta, Y. & Miura, S., 2017. Interplate coupling in and around the rupture area of the 2011 Tohoku earthquake (M9.0) before its occurrence based on terrestrial and seafloor geodetic observations, in *Int. Symp. Geodesy for Earthquake and Natural Hazards (GENAH),* pp. 11–19, Springer International Publishing, Cham.

Kano, M., Nagao, H., Ishikawa, D., Ito, S.-I., Sakai, S., Nakagawa, S., Hori, M. & Hirata, N., 2017. Seismic wavefield imaging based on the replica exchange Monte Carlo method, *Geophys. J. Int.,* **208**(1), 529–545.

Kitagawa, G., 1993. A Monte Carlo filtering and smoothing method for non-Gaussian nonlinear state space models, Technical Report, 462, Institute of Statistical Mathematics Research Memorandum.

Kitagawa, G., 1996. Monte Carlo filter and smoother for non-Gaussian nonlinear state space models, *J. Comput. Graph. Stat.,* **5**(1), 1–25.

Koketsu, K., Miyake, H. & Suzuki, H., 2012. Japan integrated velocity structure model version 1, in *Proceedings of the 15th World Conference on Earthquake Engineering,* 1773, Lisbon, Portugal.

Laske, G., Masters, G., Ma, Z. & Pasyanos, M., 2013. Update on CRUST1.0—a 1-degree global model of Earth's crust, *Geophys. Res. Abstracts,* 15, Abstract EGU2013-2658.

Malinverno, A. & Briggs, V.A., 2004. Expanded uncertainty quantification in inverse problems: hierarchical Bayes and empirical Bayes, *Geophysics,* **69**(4), 1005–1016.

Metropolis, N., Rosenbluth, A.W., Rosenbluth, M.N., Teller, A.H. & Teller, E., 1953. Equation of state calculations by fast computing machines, *J. Chem. Phys.,* **21**(6), 1087–1092.

Minson, S., Simons, M. & Beck, J., 2013. Bayesian inversion for finite fault earthquake source models I—theory and algorithm, *Geophys. J. Int.,* **194**(3), 1701–1726.

Minson, S.E., Murray, J.R., Langbein, J.O. & Gomberg, J.S., 2014. Real-time inversions for finite fault slip models and rupture geometry based on high-rate GPS data, *J. geophys. Res.,* **119**(4), 3201–3231.

Nakata, R., Hino, H., Kuwatani, T., Yoshioka, S., Okada, M. & Hori, T., 2017. Discontinuous boundaries of slow slip events beneath the Bungo Channel, southwest Japan, *Sci. Rep.,* **7**(1), 6129, doi:10.1038/s41598-017-06185-0.

Piana Agostinetti, N., Giacomuzzi, G. & Malinverno, A., 2015. Local three-dimensional earthquake tomography by trans-dimensional Monte Carlo sampling, *Geophys. J. Int.,* **201**(3), 1598–1617.

Ragon, T., Sladen, A. & Simons, M., 2018. Accounting for uncertain fault geometry in earthquake source inversions—I: theory and simplified application, *Geophys. J. Int.,* **214**(2), 1174–1190.

Rosenblatt, M., 1956. Remarks on some nonparametric estimates of a density function, *Ann. Math. Stat.,* **27,** 832–837.

Ryberg, T. & Haberland, C., 2019. Bayesian simultaneous inversion for local earthquake hypocentres and 1-D velocity structure using minimum prior knowledge, *Geophys. J. Int.,* **218**(2), 840–854.

Segall, P., 2010. *Earthquake and Volcano Deformation,* Princeton University Press.

Shimizu, K., Yagi, Y., Okuwaki, R. & Fukahata, Y., 2021. Construction of fault geometry by finite-fault inversion of teleseismic data, *Geophys. J. Int.,* **224**(2), 1003–1014.

Smith, W. & Wessel, P., 1990. Gridding with continuous curvature splines in tension, *Geophysics,* **55**(3), 293–305.

Swendsen, R.H. & Wang, J.-S., 1986. Replica Monte Carlo simulation of spin-glasses, *Phys. Rev. Lett.,* **57**(21), 2607.

Vasyura-Bathke, H., *et al.*, 2020. The Bayesian earthquake analysis tool, *Seismol. Res. Lett.,* **91**(2A), 1003–1018.

Yabuki, T. & Matsu'ura, M., 1992. Geodetic data inversion using a Bayesian information criterion for spatial distribution of fault slip, *Geophys. J. Int.,* **109**(2), 363–375.

Yagi, Y. & Fukahata, Y., 2008. Importance of covariance components in inversion analyses of densely sampled observed data: an application to waveform data inversion for seismic source processes, *Geophys. J. Int.,* **175**(1), 215–221.

Yagi, Y. & Fukahata, Y., 2011. Introduction of uncertainty of Green's function into waveform inversion for seismic source processes, *Geophys. J. Int.,* **186**(2), 711–720.

Yamaguchi, T., Ichimura, T., Yagi, Y., Agata, R., Hori, T. & Hori, M., 2017. Fast crustal deformation computing method for multiple computations accelerated by a graphics processing unit cluster, *Geophys. J. Int.,* **210**(2), 787–800.

APPENDIX: FORMULATION OF A SLIP INVERSION ANALYSIS METHOD BASED ON THE SMOOTHING CONSTRAINT

We present a slip estimation method that introduces regularization based on smoothing constraints and does not distinguish explicitly the prediction and observation errors, which is used in comparisons presented in Section 4.2.1. In the likelihood function in eq. (2), instead of considering the term of the prediction errors explicitly, the observation errors and prediction errors are considered without distinguishing each other in the form of Gaussian distribution, as

$$p(\mathbf{d}|\mathbf{m},\sigma) = (2\pi)^{-N/2}||\sigma^2\mathbf{E}||^{-1/2}\exp\left[-\frac{1}{2}(\mathbf{d}-\mathbf{G}\mathbf{m})^{\mathrm{T}}(\sigma^2\mathbf{E})^{-1}(\mathbf{d}-\mathbf{G}\mathbf{m})\right]. \tag{A1}$$

Here, we consider one of the most widely used approaches, where $\mathbf{E}$ is a diagonal matrix and does not have covariance components. We assume a prior PDF with respect to the smoothness of slip distribution,

$$p(\mathbf{m}|\sigma_{\mathrm{p}}) = (2\pi)^{-P/2}||\frac{1}{\sigma_{\mathrm{p}}^2}\mathbf{\Lambda}||^{1/2}\exp\left[-\frac{1}{2}\mathbf{m}^{\mathrm{T}}(\frac{1}{\sigma_{\mathrm{p}}^2}\mathbf{L}^{\mathrm{T}}\mathbf{L})\mathbf{m}\right],$$

where $\mathbf{L}$ is a matrix corresponding to a discretized Laplacian operator, P is the rank of $\mathbf{L}^{\mathrm{T}}\mathbf{L}$, $\mathbf{\Lambda}$ is a $P \times P$ diagonal matrix that has non-zero eigenvalues of $\mathbf{L}^{\mathrm{T}}\mathbf{L}$ as its diagonal components and σ_{p} is an unknown scaling factor. Based on Bayes' theorem, the posterior PDF of the model parameters is written as

$$\begin{aligned} p(\mathbf{m}|\mathbf{d},\sigma,\sigma_{\mathrm{p}}) &= \kappa\, p(\mathbf{d}|\mathbf{m},\sigma)p(\mathbf{m}|\sigma_{\mathrm{p}}) \\ &= \kappa\,(2\pi)^{-(N+P)/2}||\sigma^2\mathbf{E}||^{-1/2}||\frac{1}{\sigma_{\mathrm{p}}^2}\mathbf{\Lambda}||^{1/2}\exp\left[-\frac{1}{2}s(\mathbf{m})\right], \end{aligned}$$

where

$$s(\mathbf{m}) = (\mathbf{d}-\mathbf{G}\mathbf{m})^{\mathrm{T}}(\sigma^2\mathbf{E})^{-1}(\mathbf{d}-\mathbf{G}\mathbf{m}) + \mathbf{m}^{\mathrm{T}}(\frac{1}{\sigma_{\mathrm{p}}^2}\mathbf{L}^{\mathrm{T}}\mathbf{L})\mathbf{m}.$$

This formulation of the posterior PDF is identical to that presented in Yabuki & Matsu'ura (1992). They introduced Akaike's Bayesian information criterion to determine the hyperparameters σ and σ_{p}. Instead, we here seek to draw samples from the joint posterior PDF of $\mathbf{m}$, σ and σ_{p} using Algorithm 1, aiming for comparison in an equivalent condition to the proposed method. To formulate the joint posterior PDF, we introduce prior distributions for the hyperparameters as

$$p(\mathbf{m},\sigma,\sigma_{\mathrm{p}}|\mathbf{d}) = \kappa'\, p(\mathbf{d}|\mathbf{m},\sigma)p(\mathbf{m}|\sigma_{\mathrm{p}})p(\sigma)p(\sigma_{\mathrm{p}}).$$

We adopt

$$p(\sigma) = p(\sigma_{\mathrm{p}}) = U(0,b),$$

where κ' is an updated normalization factor and b is a sufficiently large number. Figs 5(c) and (d) show the marginal posterior PDF for $\mathbf{m}$ obtained by integrating $p(\mathbf{m},\sigma,\sigma_{\mathrm{p}}|\mathbf{d})$ with σ and σ_{p}.